Atmos. Chem. Phys. Discuss., https://doi.org/10.5194/acp-2017-502
Manuscript under review for journal Atmos. Chem. Phys.
Discussion started: 12 June 2017

Atmospheric Chemistry and Physics Discussions

Profiling of Saharan dust from the Caribbean to West Africa, Part 2: Shipborne lidar measurements versus forecasts

Albert Ansmann[1], Franziska Rittmeister[1], Ronny Engelmann[1], Sara Basart[2], Angela Benedetti[3], Christos Spyrou[4], Annett Skupin[1], Holger Baars[1], Patric Seifert[1], Fabian Senf[1], and Thomas Kanitz[5]

[1]Leibniz Institute for Tropospheric Research, Leipzig, Germany
[2]Barcelona Supercomputing Center, Dep. of Earth Sciences, Barcelona, Spain
[3]European Centre for Medium-Range Weather Forecasts, Reading, UK
[4]National and Kapodistrian University of Athens, Dep. of Physics, Athens, Greece
[5]ESTEC, Noordwijk, The Netherlands

Correspondence to: A. Ansmann
(albert@tropos.de)

Abstract. A unique 4-week ship cruise from Guadeloupe to Cabo Verde in April-May 2013 (see part 1, Rittmeister et al., 2017) is used for an in-depth comparison of dust profiles observed with a polarization/Raman lidar aboard the German research vessel Meteor over the remote tropical Atlantic and respective dust forecasts of a regional (SKIRON) and two global atmospheric (dust) transport models (NMMB/BSC-Dust, MACC/CAMS). New options of model-observation comparisons are presented. We analyze how well the modeled fine dust (submicrometer particles) and coarse dust contributions to light extinction and mass concentration match respective lidar observations, and to what extent models, adjusted to aerosol optical thickness observations, are able to reproduce the observed layering and mixing of dust and non-dust (mostly marine) aerosol components over the remote tropical Atlantic. Based on the coherent set of dust profiles at well defined distances from Africa (without any disturbance by anthropogenic aerosol sources over the ocean) we investigate how accurately the models handle dust removal at distances of 1500 km to more than 5000 km west of the Saharan dust source regions. It was found that (a) dust predictions are of acceptable quality for the first several days after dust emission up to 2000 km west of the African continent, (b) the removal of dust from the atmosphere is too strong for large transport paths in the global models, and (c) the simulated fine-to-coarse dust ratio (in terms of mass concentration and light extinction) is too high in the models compared to the observations. This deviation is already given close to the dust sources and then increases with distance from Africa.

1 Introduction

In a companion paper (Rittmeister et al., 2017), we present Saharan dust observations over the remote tropical Atlantic Ocean between Guadeloupe (16° N, 61° W) and Cape Verde (17° N, 25° W). Dust profiles were continuously measured during a 4–week cruise with a polarization/Raman lidar aboard the German research vessel (R/V) Meteor. The transatlantic cruise over 4500 km is shown in Fig. 1 and took place from 29 April to 23 May 2013. The lidar observations were conducted in the framework of the Saharan Aerosol Long-range Transport and Aerosol-Cloud Interaction Experiment (SALTRACE) (Weinzierl et al., 2017). Dust profile observations along the main outflow route of Saharan dust towards North America with a slowly moving

Atmos. Chem. Phys. Discuss., https://doi.org/10.5194/acp-2017-502
Manuscript under review for journal Atmos. Chem. Phys.
Discussion started: 12 June 2017

Atmospheric Chemistry and Physics Discussions

ship provide a unique opportunity to check the quality of forecasts of dust predictions models, especially the dust removal parameterization. No additional continental aerosol source disturbed the lidar observations over the remote tropical Atlantic, no orographic effect influences the air flow, and frontal activity and associated large-scale lifting of air masses causing complex vertical aerosol layering is absent over the tropical Atlantic.

There is a strong need for the evaluation of dust transport models. Huneeus et al. (2011, 2016) provide an extended overview of the status of dust transport modeling and forecasting. Since mineral dust is ubiquitous and thus influences weather and climate, horizontal visibility, air quality, and human health with extreme effects during strong dust outbreaks, precise forecasting of dust events is a major issue for environmental and meteorological services and, more general, for atmospheric sciences. Significant progress has been made in dust modeling during the last ten years and a suite of regional and global dust transport models is available. However, the unpredicted record-breaking dust storm in the Eastern Mediterranean and Middle East in September 2015 as described in Mamouri et al. (2016), Solomos et al. (2016), and Gasch et al. (2017) reminds us that dust modeling systems need to be further improved to cover all aspects of dust lifting, transport, and deposition processes, even at scales of cloud and thunderstorm formation.

Aerosol Robotic Network (AERONET) sun photometer observations (Holben et al., 1998) play a strong role in dust model evaluation (see recent studies, e.g., of Scanza et al., 2015; Cuevas et. al., 2015; Ridley et al., 2016) because of the continuity of observations since decades, the easy and free access to the data, and high quality of AERONET products. However, dust column information as provided by AERONET observations is not sufficient. The life time and spread of dust on regional to intercontinental scales sensitively depends on the height at which dust is transported and also on the dust size distribution, and thus on fine and coarse dust fractions during emission and long-range travel. Per definition, particles with diameters <1 μm belong to the fine dust fraction and coarse-mode particles have diameters >1 μm. Dust removal (wet deposition and wash out, dry deposition by gravitational settling and turbulent downward mixing) is a strong function of height. Gravitational settling also sensitively depends on the simulated fine and coarse dust fractions. The same holds for dust radiative effects which are rather different for fine and coarse dust particles (Nabat et al., 2012; Ridley et al., 2016; Kok et al., 2017). Meanwhile, dust simulations are also used to estimate dust ice-nucleating particle (INP) concentrations (Hande et al., 2015; Nickovic et al., 2016). Dust cloud condensation nucleus (CCN) concentrations can be estimated as well (Mamouri and Ansmann, 2016; Hande et al., 2016). The CCN and INP number concentrations also depend on the simulated fine and coarse dust particle fractions.

Consequently, lidar observations are required for an improved evaluation of dust prediction models (Koffi et al., 2012, 2016; Mona et al., 2014; Cuevas et. al., 2015; Binietoglou et al., 2015). Polarization lidars which allow us to separate dust from non-dust aerosol profiles in terms of light extinction coefficient and mass concentration are most useful in this respect. Recently, it was shown that even fine dust and coarse dust can be distinguished (Mamouri and Ansmann, 2014, 2017) so that one of the most important modeling aspects which deals with the emitted and transported dust particle size spectrum (Kok, 2011a, b; Kok et al., 2017) can now be illuminated in model-observation comparisons.

Our study is guided by the following main question: How well can state-of-the-art dust (regional/global) forecast models (SKIRON, MACC/CAMS, NMMB/BSC-Dust, see Sect. 3) reproduce our shipborne lidar observations of light extinction and mass concentration profiles as a function of transport length from about 1500 km to more than 5000 km from the dust source

Atmos. Chem. Phys. Discuss., https://doi.org/10.5194/acp-2017-502
Manuscript under review for journal Atmos. Chem. Phys.
Discussion started: 12 June 2017

Atmospheric Chemistry and Physics Discussions

regions? A special focus is on dust removal and the question to what extend the simulated fine and coarse dust fractions are in consistency with the lidar observations? In this context, we discuss the hypothesis of Kok (2011a, b) and Nabat et al. (2012) that dust models overestimate the fine dust fraction and underestimate the coarse dust fraction.

The cruise with a state-of-the-art continuously running dust profiling lidar across the Atlantic and the comparisons with the dust forecasts gives us, in addition, the favorable opportunity to inform the broader atmospheric science community about the recent progress in dust lidar observations and data analysis methods. We present the full set of products of the recently introduced POLIPHON (Polarization Lidar Photometer Networking) method (Mamouri and Ansmann, 2014, 2017).

The paper is structured as follows: In Sect. 2, details to the ship cruise as part of our lidar networking activities are given. The POLIPHON data analysis is explained and applied to four observations of key stages of dust layering over the tropical Atlantic (see Fig. 1, cases 1-4). These four cases were introduced and discussed by Rittmeister et al. (2017). The dust models are then briefly described in Sect. 3. The lidar observations of the four cases are compared with the model results in Sect. 4. The performance of the three dust models is discussed. The new options of comparison are applied.

2 R/V Meteor cruise as part of PollyNET and lidar data analysis

The continuously operated multiwavelength polarization/Raman lidar Polly (*PO*rtab*L*le *L*idar s*Y*stem) (Engelmann et al., 2016), used in our study for dust profiling during the transatlantic cruise M96 of the German R/V Meteor, is the key instrument of the so-called OCEANET-Atmosphere platform and is installed inside a container. The OCEANET-Atmosphere platform is usually operated during north-south cruises of the German ice breaker R/V Polarstern between Bremerhaven, Germany, and Cape Town, South Africa, or Punta Arenas, Chile in spring and autumn of each year (Kanitz et al., 2011, 2013) and thus routinely observes Saharan and Patagonian dust outbreaks. The OCEANET Polly lidar is the mobile platform of the lidar network PollyNET (Baars et al., 2016) which consists of permanent and temporary continuously running automated multiwavelength lidar stations. PollyNET is part of the European Aerosol Research Lidar Network (Pappalardo et al., 2014). One of the goals of PollyNET is the built up of a small network of autonomously running dust monitoring lidar stations in Cabo Verde, Cyprus, Crete, Israel, and Tajikistan. The aim is to support dust forecast modeling and to pave the way towards lidar data assimilation into dust forecast models. It is planned to run these PollyNET stations together with AERONET sun photometer stations.

The Polly data analysis software was recently extended by introducing the POLIPHON retrieval technique. The method enables us to decompose the measured aerosol profiles, i.e., to separate vertical profiles of fine dust, coarse dust, and the non-dust aerosol component in terms of particle extinction coefficient and mass concentration. By means of the aerosol Raman lidar method (Ansmann et al., 1992) we are even able to identify and characterize the non-dust aerosol type, whether this component is, e.g., of maritime or continental origin (Mamouri and Ansmann, 2017). The new method is robust and simple (because based on single-wavelength 532 nm lidar observations only), and does not need any sophisticated particle shape model for the irregularly shaped dust particles in the data analysis. In alternative multiwavelength lidar retrievals (discussed in Mamouri and Ansmann, 2014, 2017), the dust particles are usually assumed to be spheroidal in shape which is not justified for lidar applications (Gasteiger et al., 2011; Lindqvist et al., 2014; Kemppinen et al., 2015a, b).

Atmos. Chem. Phys. Discuss., https://doi.org/10.5194/acp-2017-502
Manuscript under review for journal Atmos. Chem. Phys.
Discussion started: 12 June 2017

Atmospheric Chemistry and Physics Discussions

The retrieval of profiles of the basic particle optical properties (backscatter coefficient, extinction coefficient, lidar ratio, depolarization ratio, input for POLIPHON) from the Polly observations is described by Engelmann et al. (2016) and Baars et al. (2016). The respective results for the four cases studied here are presented in the companion paper of Rittmeister et al. (2017). In this section, we briefly describe the POLIPHON part of data analysis. The POLIPHON retrieval consists of four steps. These steps are shown in Fig. 2 (c-e). We applied the method to case 4 in Fig. 1. On 5-6 May 2013, the R/V Meteor was 600 km west of Barbados. An aged Saharan dust plume was detected between 800 and 2000 m height after 9 days of travel across the tropical Atlantic. The height profiles of the particle backscatter coefficient (Fig. 2a) and particle linear depolarization ratio at 532 nm (Fig. 2b) as presented and discussed in Rittmeister et al. (2017) are input of the POLIPHON data analysis, as mentioned.

In the first step, the vertical profiles of the particle depolarization ratio and backscatter coefficient are used to separated the dust and non-dust contributions to the measured (total) particle backscatter coefficient (Fig. 2c). Non-dust aerosol components are biomass burning smoke, anthropogenic haze (from industry, traffic, heating), rural (background) aerosol, and marine particles. A depolarization ratio of >0.31 and <0.05 indicates pure dust and pure non-dust aerosol, respectively. Depolarization ratios from 0.05–0.31 indicate mixtures of dust and non-dust aerosol and can be easily quantified by applying the classical separation technique (e.g., Sugimoto et al., 2003; Shimizu et al., 2004; Tesche et al., 2009). This basic separation technique is denoted as one-step method of the POLIPHON retrieval scheme (Mamouri and Ansmann, 2014). The solutions are shown in Fig. 2c for the dust (red) and non-dust (green) particle backscatter coefficient.

In the next step (step 2), we convert the backscatter coefficients into light-extinction coefficients. In our specific case of shipborne measurements west of Africa, we multiply the dust backscatter values with a typical extinction-to-backscatter ratio (lidar ratio) of 55 sr for, e.g., western Saharan dust (Groß et al., 2011; Tesche et al., 2011; Haarig et al., 2017a) to obtain the height profiles of the dust extinction coefficient at 532 nm. The result is shown in Fig. 2d. In the same way, the non-dust backscatter coefficients are converted to extinction coefficients. To cover the entire spectrum of possible non-dust aerosol scenarios from pure marine to pure continental aerosol, we calculate marine particle extinction coefficients by using a typical marine lidar ratio of 20 sr in the conversion (Groß et al., 2011; Rittmeister et al., 2017) and a continental (non-dust) aerosol extinction coefficient by taking a typical lidar ratio of 50 sr for anthropogenic aerosols at 532 nm (Müller et al., 2007a). All three extinction profiles (dust in red, marine in blue, and anthropogenic in green) are shown in Fig. 2d in this way.

Afterwards (step 3), we check, whether the sum of marine and dust extinction profiles or the sum of anthropogenic aerosol and dust extinction profiles approximately agrees with the particle extinction profile at 532 nm as independently obtained with the Raman-lidar method (see Mamouri and Ansmann, 2017, for more details). As can be seen in Fig. 2d, the Raman lidar solution for the total particle extinction coefficient (black curve) is already close to the dust extinction profile in the Saharan air layer (SAL) and close to the marine extinction coefficient in the marine aerosol layer (MAL) below the SAL. Raman lidar solution for the extinction coefficients are determined from nitrogen Raman backscatter profiles and uncertainties in the correction of the laser-beam to receiver-field-of-view overlap correction prevent a trustworthy determination of the extinction profile at heights below 600 m. All other lidar profiles shown in Fig. 2 (a-e) are trustworthy almost down to heights close to the surface because they are calculated from lidar signal ratios so that the overlap impact widely cancels out.

Atmos. Chem. Phys. Discuss., https://doi.org/10.5194/acp-2017-502
Manuscript under review for journal Atmos. Chem. Phys.
Discussion started: 12 June 2017

Atmospheric Chemistry and Physics Discussions

As outlined in detail in Rittmeister et al. (2017), the identification of aged smoke in the SAL after long-range transport over more than 5000 km within 9–10 day is complicated because fire smoke particles may significantly grow by water uptake during long-range transport and, as a consequence, change their optical properties (Müller et al., 2007b). The lidar ratio of fresh smoke may be as high as 50–70 sr, but can decrease significantly, e.g., to values around 30 sr (as is the case here) after such a long travel over more than a week. Thus, it is not clear in Fig. 2d whether the small remaining non-dust contribution to light extinction in the SAL is caused by marine or aged smoke particles or a mixture of both.

We repeated the procedure of the identification of the non-dust aerosol component for the other three cases. The results are shown in Fig. 3. Again, the Raman-lidar profile of the total particle extinction coefficient is already close to the dust extinction profile in the SAL in cases 1 and 3, and indicates pure marine aerosol conditions in the marine layer below the SAL in case 3. The weak non-dust aerosol contribution to total light extinction in the SAL (case 3) may indicate the presence of marine particle (lidar ratio of 20sr) or of aged smoke (lidar ratio of 30 sr). In case 2, we clearly observed a mixture of dust and smoke and other anthropogenic aerosol particles (causing a lidar ratio of 50 sr or an even slightly higher value) in the SAL at heights $>$1.8 km. The particle extinction profile obtained from the Raman lidar measurement and the dust extinction profile are only close to each other for the lowest part of the SAL. The Raman-lidar extinction values are again close to the marine extinction coefficients in the MAL in case 2. In the model-observation comparison in Sect. 4.1, we ignore the smoke and haze impact in the SAL (case 2) for simplicity, and concentrate on marine and dust particle extinction and mass concentration profiles. Marine particles dominated in the MAL and desert dust in the SAL.

In the final step (see Fig. 2e), we convert the extinction coefficients for dust, marine, and anthropogenic aerosol into respective mass concentration values by using appropriate extinction-to-volume conversion factors given in Mamouri and Ansmann (2017). The respective conversion factors were obtained from multi-year AERONET sun photometer observations and from field campaigns with lidar/photometer combinations. In addition, we assume particle densities of 1.2 g cm^{-3} (marine), 1.55 g cm^{-3} (continental pollution) and 2.6 g cm^{-3} (dust) in the extinction-to-mass conversion.

By means of a new option, denoted as 2-step method in the POLIPHON retrieval framework, we can even separate fine dust and coarse dust contributions to the total dust backscatter and extinction coefficients and thus estimate fine and coarse dust mass concentrations. Details can be found in Mamouri and Ansmann (2017). The method makes use of the fact that fine dust and coarse dust show different depolarization ratios of 0.14–0.18 (fine dust, 532 nm) and 0.35-0.39 (coarse dust, 532 nm). The fine and coarse dust backscatter, extinction, and mass concentration profiles for the measurement example in Fig. 2 are shown in Fig. 4. The method assumes vertically homogeneous dust properties within the SAL and thus a height-independent dust size distribution so that the ratio of fine dust to coarse dust extinction coefficient and mass concentration is also height independent. The obtained fine dust and coarse dust profiles of our cases 1-4 are in full agreement with the shipborne sun photometer observations of fine dust and coarse dust AOT at 500 nm on the four days.

The uncertainties in the lidar products are indicated by error bars in Figs. 2 to 4. These error bars include the uncertainty in the separation of dust and non-dust aerosol components, in the assumed lidar ratios in the retrieval of the extinction coefficients, and in the extinction-to-mass conversion factors. Typical overall uncertainties in all presented parameters are discussed in Mamouri and Ansmann (2017).

Atmos. Chem. Phys. Discuss., https://doi.org/10.5194/acp-2017-502
Manuscript under review for journal Atmos. Chem. Phys.
Discussion started: 12 June 2017

Atmospheric Chemistry and Physics Discussions

3 Atmospheric modeling tools

3.1 SKIRON

The SKIRON modeling system is an integrated limited area modeling system (a regional dust prediction systems) developed at the National and Kapodistrian University of Athens (Kallos et al., 2007; Astitha et al., 2008; Spyrou et al., 2010) in the framework of the nationally and European Union (EU) funded projects SKIRON, Mediterranean Dust Experiment (MEDUSE), Atmospheric Deposition and Impact on the Open Mediterranean Sea (ADIOS), and recently Climate Change and Impact Research (CIRCE) and Marine Renewable Integrated Application Platform (MARINA). The SKIRON system simulates the dust cycle (uptake, transport, deposition and its impacts on radiation) and provides dust load and deposition forecasts (available at http://forecast.uoa.gr/dustindx.php). The name SKIRON (one of the eight gods of winds) is taken from the Greek mythology.

A contrasting feature to the other two models used here is the formulation of the source function (characterization of accumulated sediments, soil texture, porosity, bulk density, composition, soil moisture, and soil particle size distribution). SKIRON uses the soil texture database developed by Miller and White (1998) which, in turn, is based on the US Department of Agriculture's State Soil Geographic Database. The atmospheric model is based on the ETA/National Centers for Environmental Prediction (NCEP) model but is heavily modified to include state-of-the-art parameterization schemes for meteorological and desert dust processes (see Spyrou et al., 2010, for details). Recently the model was updated to use the RRTMG (Rapid radiative transfer model for global circulation models) radiative transfer scheme (Iacono et al., 2008) in order to calculate the radiative feedback of dust particles in the atmosphere (Spyrou et al., 2013).

The particle size distribution of atmospheric dust is represented by eight size bins with effective radii of 0.15, 0.25, 0.45, 0.78, 1.3, 2.2, 3.8, and 7.1 μm (Spyrou et al., 2010). Table 1 shows the size bins (radius classes) used in SKIRON and for comparison the particle radius classes implemented in the other two models described below.

The simulated dust mass concentration profiles were provided by the University of Athens (from the operational dust forecasting system) for the nearest model grid point to the R/V Meteor and nearest time step to the lidar observations (cases 1–4). The particle extinction coefficients for 550 nm were then calculated from the simulated size-class-resolved mass concentrations by using the effective radius per size class representing the standard size of the particles of each of the eight classes, the dust density of 2.6 g cm^{-3}, and literature values of dust refractive indices and dust extinction efficiencies for the given eight effective radii. Spherical dust particles are assumed in the calculation of the extinction coefficients. A detailed description of the computations of dust extinction coefficients from the modeled dust mass concentrations is given by Tegen and Lacis (1996), Pérez et al. (2006), and Spyrou et al. (2013).

3.2 MACC/CAMS

MACC (Monitoring Atmospheric Composition and Climate) was developed within the framework of an European Union (EU) project (*http://www.gmes-atmosphere.eu/about/project/*) which was coordinated by ECMWF (European Centre for Medium-range Weather Forecasts, Reading, United Kingdom). MACC activities are now carried on under the Copernicus Atmosphere Monitoring Service (CAMS). The simulation system MACC/CAMS combines state-of-the-art atmospheric model-

ing with Earth observation data to provide information services covering European air quality, global atmospheric composition, climate forcing, the ozone layer and UV, solar energy, and emissions and surface fluxes. The MACC/CAMS simulation tool gets input data from satellites, in situ measurements and information about aerosol emissions and fires. The anthropogenic emissions are based on established inventories. Two main global MACC/CAMS products are analyses and forecasts of aerosols (*http://www.gmes-atmosphere.eu/*). Details to this complex simulation tool can be found in Morcrette et al. (2009), Benedetti et al. (2009), Wagner et al. (2015), Marécal et al. (2015), and Cuevas et. al. (2015).

The MACC/CAMS aerosol parameterization is based on the LOA/LMD-Z (Laboratoire d'Optique Atmosphérique/Laboratoire de Météorologie Dynamique-Zoom) model (Reddy et al., 2005). MACC/CAMS considers five types of tropospheric aerosols: sea salt, dust, organic and black carbon, and sulphate aerosols. Prognostic aerosols of natural origin such as mineral dust and sea salt are described using three size bins. For dust, the size (radius) classes are from 0.03–0.55 μm, 0.55–0.9 μm, and from 0.9–20 μm (see Table 1), whereas for sea salt, the bin limits are at 0.03, 0.5, 5 and 20 μm (Morcrette et al., 2009). For the production of desert dust in the ECMWF model, a formulation of the source was implemented following the approach of Ginoux et al. (2001).

MODIS (Moderate Resolution Imaging Spectroradiometer) observations of aerosol optical thicknesses (AOT) are assimilated into the model (Benedetti et al., 2009). The AOT used in the MACC/CAMS simulations in 2013 was retrieved by means of a MODIS aerosol analysis scheme which consisted of two entirely independent algorithms, one for deriving aerosols over land (for dark surfaces) and the second for aerosols over ocean (Remer et al., 2005). AOT information for the bright dust source regions were partly not available or highly uncertain. The MACC/CAMS AOT observation operator derives the optical depth based on precomputed aerosol optical properties and model relative humidity for the aerosol species mentioned above. After assimilation, the model output represents the best statistical compromise between the model background (forecast running without assimilation) and observations.

The MACC reanalysis was stopped in 2012 so that reanalysis products are not available for 2013. Therefore, the operational (forecast) runs for 2013 were used in our study. Data sets of particle mass concentrations were downloaded from the ECMWF data server (MACC, 2016). Aerosol products are available for a fixed grid with resolution of 1.125°. We selected the data sets for the nearest grid points to the position of R/V Meteor and 00:00 UTC (cases 2-4) and 04:00 UTC (case 1, 23 May 2013). The model resolution is $0.8° \times 0.8°$ with 60 vertical levels.

As mentioned, dust mass concentrations are available for three radius classes.The radius class from 0.03–0.55 μm defines the fine dust fraction, the two other size classes belong to the coarse mode. Morcrette et al. (2009) state that the size bins are chosen such that the mass concentration percentages are 10% for the fine dust class, and 20% and 70% for the two coarse dust size bins during emission. We calculated the particle extinction coefficients at 550 nm by dividing the MACC/CAMS fine, coarse and total dust mass concentrations by extinction-to-volume conversion factors of 0.21×10^{-12} Mm (fine dust), 0.81×10^{-12} Mm (coarse dust), 0.64×10^{-12} Mm (total dust), and 0.65×10^{-12} Mm (marine aerosol) (Mamouri and Ansmann, 2017), respectively, and by the particle density. MACC/CAMS assumes a particle density of 2.6 g cm^{-3} for mineral dust and of 1.2 g cm^{-3} for marine particles. The used extinction-to-volume conversion factors derived from extended AERONET studies at Morocco, Cabo Verde, and Barbados (Mamouri and Ansmann, 2017) are in full agreement with the defined mass specific

extinction coefficients linking the microphysical and the optical properties (at 550 nm) in the MACC/CAMS model given in Benedetti et al. (2009). As in the case of SKIRON (and of NMMB/BSC-Dust, see text below), the MACC/CAMS fine dust class (0.03–0.55 μm radius) includes particles with radii exceeding 0.5 μm so that a weak overestimation of the fine-mode dust extinction coefficients of the order of 10% must be taken into account in the discussions of the results in the next section.

3.3 NMMB/BSC-Dust

The NMMB/BSC-Dust model (NMMB: Nonhydrostatic Multiscale Model on the B Grid, BSC: Barcelona Supercomputing Center) is the mineral dust module of the NMMB-MONARCH (MONARCH: Multiscale Online Nonhydrostatic AtmospheRe CHemistry) (Pérez et al., 2011; Haustein et al., 2012; Jorba et al., 2012; Spada et al., 2013; Badia and Jorba, 2014; Basart et al., 2016; Di Tomaso et al., 2017) designed and developed at BSC (Barcelona Supercomputing Center) in collaboration with NOAA NCEP (NOAA: U.S. National Oceanic and Atmospheric Administration, NCEP: National Centers for Environmental Prediction), and the NASA Goddard Institute for Space Studies. The dust model is online coupled with the non-hydrostatic NMMB model (Janjic et al., 2011, and references therein), which is able to increase the model horizontal resolution up to 1 km. The NMMB/BSC-Dust model provides operational forecast over regional (North Africa, Middle East, Europe) and global domains, and it has been selected by the World Meteorological Organization (WMO) as the operational model for the Barcelona Dust Forecast Center (http://dust.aemet.es/), the first WMO regional center specialized in atmospheric sand and dust forecast. Additionally, the model is participating in the WMO (Sand and Dust Storm Warning Advisory and Assessment System, SDS-WAS, https://sds-was.aemet.es/) and ICAP (International Cooperative for Aerosol Prediction, http://www.nrlmry.navy.mil/aerosol/icap.1135.php) model intercomparison exercises.

The NMMB/BSC-Dust model assumes a viscous sublayer between the smooth desert surface and the lowest model layer (Janjic, 1994; Nickovic et al., 2001), and its dust emission caused by surface and turbulence winds are physically-based on an emission scheme which explicitly considers saltation and sandblasting processes (White, 1979; Marticorena and Bergametti, 1995; Marticorena et al., 1997). The model uses soil texture data from the hybrid STATSGO-FAO (STATGO: State soil geographic data base, FAO: Food and Agriculture Organization of the United Nations) soil map and land use data of the USGS (United States Geological Survey). According to the criteria used in Tegen et al. (2002), the model considers 4 soil populations (i.e. clay, silt, fine-medium sand and coarse sand). The dust vertical flux is distributed following D'Almeida et al. (1987) and then distributed over each of the 8 dust size transport bins (0.1-10 μm, see Table 1). Mineral dust source areas are defined through the topographic preferential source approach (Ginoux et al., 2001) and the National Environmental Satellite, Data, and Information Service (NESDIS) vegetation fraction climatology (Ignatov and Gutman, 1998). The model solves the mass balance equation and includes parameterizations for the gravitational settling and dry deposition at the first layer (Zhang et al., 2001), and wet deposition by sub-cloud and in-cloud scavenging from convective and stratiform clouds (Betts, 1986; Betts and Miller, 1986; Janjic, 1994; Ferrier et al., 2002). The model has been evaluated at regional and global scales (Pérez et al., 2011; Haustein et al., 2012; Gama et al., 2015; Binietoglou et al., 2015; Huneeus et al., 2016; Basart et al., 2016) showing the ability of the model to reproduce the dust cycle.

Atmos. Chem. Phys. Discuss., https://doi.org/10.5194/acp-2017-502
Manuscript under review for journal Atmos. Chem. Phys.
Discussion started: 12 June 2017

For the current intercomparison exercise, a global experiment with $1.4° \times 1°$ horizontal resolution and 40 hybrid layers is considered. The simulated dust distributions consist of daily (24 hours of forecast) runs for 25 April to 23 May 2013. The NCEP/FNL final analyses (at $1° \times 1°$) at 0 UTC are used as initial meteorological conditions. The model does not include a dust data assimilation system. The initial state of the dust concentration is defined by the 24-h forecast of the previous-day model run. Only in the 'cold start' of the model, concentration is set to zero. In this contribution, simulations were carried out with the operational RRTM (Rapid Radiative Transfer Model) radiation scheme (Mlawer et al., 1997) which allows feedback between dust and radiation. Simulated fields of dust mass (per bin of the model) with a temporal resolution of three hours are used to obtain the bilinear temporal and spatial interpolated simulated profiles of the NMMB/BSC-Dust model following the transatlantic path (Fig. 1). Dust extinction coefficients at 550 nm are computed from the simulated dust mass concentration profiles in the same way as described in Sect. 3.1 for the SKIRON simulations.

4 Comparisons

4.1 Marine and dust aerosol profiles: MACC/CAMS simulations vs lidar observations

MACC/CAMS provides forecasts for a variety of aerosol species, and therefore allows us to compare vertical distributions of the main aerosol components (marine and dust particles) we observed during the R/V Meteor cruise. In Fig. 5, simulated and observed height profiles of the particle extinction coefficient of marine particles and Saharan dust are shown for the four selected key scenarios (cases 1-4 in Fig. 1) of dust layering over the tropical Atlantic. We removed the smoke and haze contribution from the lidar-derived non-dust extinction profile in the SAL (above 2 km height) in case 2. The non-dust extinction contribution in the SAL in cases 3 and 4 may be caused by aged smoke, but we cannot exclude that this aerosol is of marine origin after long-range transport over the Atlantic. As described in Rittmeister et al. (2017), the lofted dust in the SAL observed on 5 May 2013 (case 4) traveled about 9 days across the Atlantic (4300 km) before reaching the research vessel at 53°W at relatively low heights. The dust air masses observed on 9-10 May (case 3) needed 5 days for the 3300 km travel from the west coast of Africa to the R/V Meteor. The dust layer on 14-15 May (case 2) and 23 May (case 1) needed 3 days and one day across the Atlantic (1700 km), respectively, before reaching the lidar site. The strong dust layers observed on 23 May at Cabo Verde (case 1) were advected directly from desert areas north of 15°N so that the impact of anthropogenic haze and biomass burning smoke was low.

As can be seen in Fig. 5, the dust load and vertical distribution is well simulated in cases 1 and 2. There is very good agreement regarding both, the marine aerosol profile and the dust profiles in case 2. The model results deviate considerably from the lidar observations in cases 3 and 4, disregarding the uncertainty regarding the non-dust (marine or smoke/haze) extinction contribution in the SAL. Before discussing the differences between the observations and the model results in more detail, it should be emphasized that the dust layering observed with lidar remained unchanged over hours (Rittmeister et al., 2017) in all four cases so that we can conclude that the lidar observations are representative for the dust conditions of a larger area around the R/V Meteor (100 km$\times$100 km) and thus appropriate for comparison with the modeling results. The variability in the model dust profiles was checked by comparing all 9 profiles (8 around the ship and the one shown in Fig. 5). The modeled

dust profiles varied within 20–30% (standard deviation, case 1), 10–20% (case 2), 50-80% (case 3), and 20-30% (case 4) for the height range of the SAL.

The lidar-derived overall (marine + dust) AOT values for cases 1–4 are 0.63, 0.26, 0.11, and 0.11, respectively, and close to the ones obtained by integrating the MACC/CAMS extinction profiles of marine aerosols and dust particles over the vertical column and adding both column values. MACC/CAMS AOTs are 0.54 in case 1, 0.28 in case 2, 0.12 in case 3, and 0.15 in case 4. As mentioned above, MACC/CAMS was assimilating MODIS AOT data in 2013. As shown in Fig. 5, the strong underestimation of the dust load in cases 3 and 4 is compensated by unrealistic profiles for the marine aerosol to match the MODIS AOT. Case 4 shows a strong marine layer up to 3 km and a marine AOT of 0.16, whereas the reality is reflected in the lidar observations with a top height of the marine boundary layer (MBL) at 1 km height and an overall (MBL and free tropospheric) marine AOT of 0.06. The lidar indicates marine particles mainly below 1 km height and marine AOT of 0.09, 0.1, 0.05, and 0.06 for cases 1–4, respectively. MACC/CAMS simulates marine AOTs of 0.15-0.16 for case 1,2 and 4, and about 0.1 for case 3. Thus, the quality of the dust forecast clearly decreases with distance from Africa and increasing dust travel time. However, MACC/CAMS predicts the SAL height range (from bottom to top) very well in cases 1–3.

Efforts are undertaken to improved global dust cycle modeling by assimilation of higher-level spaceborne AOT products into the forecast models (see, e.g., Huneeus et al., 2012; Di Tomaso et al., 2017; Escribano et al., 2017). The consideration of MODIS (Deep Blue) AOT products is promising. It is expected that the dust forecasts, especially over continents (including the bright dust source regions) will be significantly improved.

Recently, Haarig et al. (2017b) showed that the dust lidar retrieval may be slightly affected by enhanced light depolarization, when wet, spherical sea salt particles get dried and then become almost cubic in shape. This occurs usually at the top of the MBL where the relative humidity drops from values around 80% to <50% in the free troposphere. The retrieved dust mass concentration is then too high when assuming spherical marine particles and a marine depolarization ratio of 0.02–0.03. Cubic sea salt particles can cause particle depolarization ratios of 0.1–0.15. The dry marine particle effect may be responsible for the small peaks in the dust extinction profiles at MBL top coinciding with the SAL bottom in cases 1 and 2. The effect is however in the 5-10% range regarding the underestimation of the marine AOT and thus can be neglected in our model-observation comparisons.

4.2 Dust mass profiles: MACC/CAMS, NMMB/BSC-Dust, and SKIRON simulations vs lidar observations

In Fig. 6, we compare the dust mass concentrations obtained with the three models with the respective lidar observations. NMMB/BSC-Dust simulations are available for cases 2–4 only. As a main result, good agreement with the lidar observations were obtained in case 2 (MACC/CAMS, NMMB/BSC-Dust). SAL top and base heights were well predicted in cases 2 and 3. However, the two global models considerably underestimate the dust load in cases 3 and 4. The vertically-integrated dust mass concentrations (numbers are given in Fig. 6) are a factor of 2 (case 3, 3300 km west of Africa) and 3 (case 4, 4300 km west of Africa) smaller than the measured ones in the case of the MACC/CAMS and NMMB/BSC-Dust simulations. We analyzed METEOSAT satellite observations for the potential impact of wet deposition and found that, except for case 4, wet deposition can be excluded.

Atmos. Chem. Phys. Discuss., https://doi.org/10.5194/acp-2017-502
Manuscript under review for journal Atmos. Chem. Phys.
Discussion started: 12 June 2017

Atmospheric Chemistry and Physics Discussions

In contrast to the column mass values obtained with the global models, the ones simulated with the regional model SKIRON are in good agreement with the lidar values. However, a systematic shift of the dust maximum mass concentration towards lower heights (compared to the lidar profiles) is observed in the SKIRON profiles in all of the four observational cases. As discussed in Sect. 4.3, the ratio of fine dust to coarse dust mass fraction is set constant throughout the simulation period in the SKIRON model and the fine-to-coarse dust fraction is generally lower in SKIRON simulations than in the forecasts obtained with the global models (NMMB/BSC-Dust, MACC/CAMS). As a result of the higher coarse dust fraction, gravitational settling obviously has a higher impact on the dust profile simulated with the regional SKIRON model.

It is impossible to identify the reason for the obviously too strong removal of dust in these complex atmospheric transport models. Too many sources for uncertainties (including numerical losses in the complex mathematical treatments) exist. Many experimental and empirically derived constants are used in the source/emission, transport, and deposition parameterizations so that simple conclusions concerning the reasons for the found uncertainties can not be drawn. The differences in forecasts can be large. Huneeus et al. (2016) compared simulations of five different models in the case of a strong Saharan dust outbreak towards northern Europe and found differences between the largest and the smallest dust emissions of the order of a factor of 10. As Kok et al. (2014a, b) mentioned, the simulations of the global atmospheric dust cycle are hindered by the empirical nature of the presently widely used dust emission (or source) parameterizations in weather and climate models. These parameterizations are generally tuned to reproduce the current dust cycle (for given present climate conditions, global circulation pattern, land use, and surface characteristics), and thus can introduce large uncertainties for specific, individual, regional meteorological conditions and individual dust outbreak scenarios.

A too strong dust removal effect was observed in many studies (e.g., Kim et. al., 2014; Mona et al., 2014; Binietoglou et al., 2015). Kim et. al. (2014) found a systematic underestimation of the dust load by a factor of 2 from the African coast downwind to Barbados according to the satellite observations (MODIS and MISR: Multi-angle Imaging SpectroRadiometer), whereas the five involved models produced a decay by a factor of roughly 4–10 from the west coast of Africa to 60°W. They also found large intermodel diversities. The retention of the coarse mode particles was also noticed in recent airborne Saharan dust studies by Ryder et al. (2013) and Weinzierl et al. (2017).

One possible reason for the too strong dust removal in the models was discussed in part 1 (Rittmeister et al., 2017). The R/V Meteor lidar observations, the SALTRACE observations at Barbados, as well as spaceborne lidar measurements (CALIOP: Cloud Aerosol Lidar with Orthogonal Polarization) over the tropical Atlantic suggest that other processes besides gravitational settling of dust must be active in the SAL, and weaken the dust removal strength caused by fall out of dust particles (Ulanowski et al., 2007; Nicoll et al., 2011; Yang et al., 2013; Colarco et. al., 2003; Gasteiger et al., 2017; Haarig et al., 2017a). During SALTRACE, the lidars generally observed an almost height-independent vertical profile of the dust-related particle depolarization ratio within the SAL which indicates well-mixed conditions rather than an accumulation of larger particles in the base region of the SAL as would be the case as a result of gravitational settling. A higher amount of coarse particles in the lower part of the SAL would lead to a systematic decrease of the particle depolarization ratio from SAL base to top. Gasteiger et al. (2017) argue that absorption of solar radiation introduce turbulent mixing of dust within the SAL which weakens the pure sedimentation-based removal effect. Yang et al. (2013) discusses the possibility that different shapes of small (less

irregularly shaped) and large particles (more irregularly shaped) may have an impact on falling speed and thus the vertical dust distribution. Ulanowski et al. (2007) observed that dust layers have an impact on the atmospheric electric field, and argue that dust particles can become charged (when colliding with themselves or the underlying surface), and may be vertically aligned in the electric field, and conclude that these charging effect influence the downward transport of dust.

In the companion paper of Rittmeister et al. (2017), it is further mentioned that the observed particle extinction coefficient in the SAL was always 50–100 Mm^{-1} (cases 2–4) and the particle depolarization ratio showed vertically homogeneous dust conditions. In addition, the wavelength dependence of particle extinction and backscattering, which remained unchanged within the SAL during the long-range tranport, does not indicate a significant change in the dust size characteristics in the SAL during the travel across the Atlantic. If gravitational settling would dominate, we should see a clear decrease of the dust extinction coefficient with time, a decrease of the depolarization ratio from SAL base to SAL top as discussed in part 1 (Rittmeister et al., 2017), and also an increase of the wavelength dependence of the optical properties in the SAL.

4.3 Fine-mode and coarse-mode dust profiles: simulation vs observation

We compare, to our knowledge for the first time, fine dust and coarse dust profiles derived from the lidar observations with simulated ones. Huneeus et al. (2011) emphasized the need for height-resolved observations of dust-size-characterizing parameters. In their overview and review paper the authors stated that the dust extinction coefficient and the corresponding dust AOT-related radiative effects are sensitively controlled by the amount of occurring fine dust particles due to their higher extinction efficiency, whereas coarse dust dominates the surface concentration, deposition, and removal. In a recent study, Kok et al. (2017) emphasize in detail the consequences of a not-well modeled dust size distribution and abundance for the global energy balance through direct interaction of dust with radiation. As mentioned, the indirect climate effect of dust through interaction with clouds is also affected if the dust size distribution and load and thus estimates of CCN and INP concentrations are wrong in the forecast models.

Kok (2011a, b) stimulated a discussion on the dust mobilization parameterization which may have strong consequences for the fine-mode and coarse-mode fractions of the atmospheric dust burden. Dust emission according to the theory of saltation and sandblasting predict that the size of emitted dust aerosols decreases with wind speed (Shao, 2001, 2004; Alfaro and Gomes, 2001), whereas the brittle fragmentation theory of dust emission predicts that the emitted dust particle size distribution is independent of the wind speed (Kok, 2011b). Dust emission following the saltation/sandblasting parameterization leads to a size distribution with a comparably strong fine dust fraction and a less pronounced coarse dust fraction. In contrast, according to the brittle fragmentation theory larger coarse dust (particles with diameters exceeding 5 μm) dominates the emitted size spectrum (Kok, 2011a, b; Kok et al., 2017). Consequently, the fine fraction is likewise low in the case of brittle fragmentation parameterization. In fact, the emitted dust spectrum contains a factor of 10 to 20 higher amount of fine dust mass for particles with sizes (diameters) of 500 nm in the case of the saltation parameterization compared to brittle fragmentation paramaterization. Opposed to that, the coarse dust mass concentration is a factor of 2–7 lower in the case of the saltation parameterization compared to the alternative approach for particle with diameters around 10 μm (Kok, 2011a). A discussion on strong variations

and changes in the Saharan dust size distribution observed with aircraft close to the Saharan dust emission zones in fresh and moderately aged dust layers and aged dust layers over the Canary Islands is given by Ryder et al. (2013).

Figures 7 and 8 now show the comparisons between the modeled and observed fine dust and coarse dust extinction and mass concentration profiles. As we mentioned above, our lidar observations are in full agreement with the 500 nm AOT fine dust fractions observed with sun photometer (of about 0.2) during the cruise, and thus reflect very well the true fine-to-coarse dust extinction and mass conditions. The aircraft observation of the dust size distribution during the SALTRACE transfer flights from Africa to the Caribbean on 17-22 June 2013 also reveal fine mode fractions (for 532 nm extinction) of 0.25 in the Cabo Verde region and 0.2 over Barbados (Weinzierl et al., 2017). As can be seen in Fig. 7, the fine dust mass concentration is well simulated with the NMMB/BSC-Dust model, but the coarse dust fraction is systematically underestimated. Because the optical efficiency of small particles is much higher than of large particles the contrast between fine and coarse dust contributions is much larger in terms of particle extinction coefficient. The fine dust and coarse dust contributions to light extinction computed from the modeled mass concentrations (by means Mie scattering calculations, considering the eight size bins) are almost equal (1:1) in the case of the NMMB/BSC-Dust simulations, whereas the lidar observations reveal a much lower value of fine-to-coarse dust light extinction ratio (about 1:4). The simulated contributions of fine dust to total dust light extinction coefficient are strongly overestimated. It should be emphasized that the simulated size distribution (eight size classes) in the NMMB/BSC-Dust model consist of a pronounced coarse mode and the fine dust contribution originate from the particles in the small-particle wing (size classes 1-3).

The results are similar in the case of the MACC/CAMS simulations in Fig. 8 (top). The ratio of fine-to-coarse dust extinction coefficient steadily increases with transport distance from Africa. The fine dust contribution to light extinction is strongly overestimated, especially in cases 3 and 4 when compared to the lidar observations. In contrast, SKIRON (Fig. 8 (bottom)) is in comparably good agreement with the lidar observations. However, this result is obtained by setting the fine-to-coarse dust mass ratio to a constant value throughout the simulations.

As already mentioned in Sect. 4.2, it is impossible to identify the reason for the differences between the observation and the simulations of the fine-to-coarse dust fraction. There are so many sources of uncertainties in the complex parameterizations in the models that simple, straight forward conclusions can not be drawn.

5 Conclusions

We used the unique opportunity of a 4-week ship cruise across the tropical Atlantic Ocean with detailed lidar profiling of the SAL dust optical properties to intensively compare the observations with respective products of three dust forecasting models. New options of comparison were introduced. We found good to reasonable agreement between simulations and observed dust profiles within the transport range of about 2000 km downwind of Africa and thus about 2500-4000 km west of the Saharan dust source regions. The quality of the simulation results decreased with distance from the source regions. Height profiles of observed and simulated mixtures of marine and dust profiles provided some insight into the value of AOT assimilation to increase forecast quality. The simulated ratios of fine to coarse dust light extinction and mass concentration deviated partly

strongly from the observations (too high in the model) and increased with transport path length. The complex model structures (including the differences regarding the meteorological drives in the three models) and the used large set of empirical constants in the emission, transport, and deposition parameterizations made it however impossible to identify the reasons for the observed partly systematic biases in the model forecasts.

More airborne and lidar observations close to dust sources such as presented by Ryder et al. (2013) and in the near range of the long-range transport regime (case 1 in our discussion) are needed to improve our knowledge about dust emissions and the size spectrum during dust release. More observations are also needed to study long-range transport and dust removal (cases 2-4) and to clarify the role of different mechanisms which are potentially able to prolong the atmospheric lifetime of coarse dust particles.

The article showed the usefulness of advanced polarization lidar studies to support and improve dust modeling efforts. As an outlook, it must be a clear goal to establish ground-based polarization lidar networks, to combined ground-based and space-borne lidar observations as a contribution to global dust monitoring, and to use these dust profiling data in efforts of assimilation of observations data into dust forecast models.

6 Data availability

The R/V Meteor lidar data are available at TROPOS upon request (info@tropos.de). The NMMB/BSC-Dust dust profiles are available upon request (http://www.bsc.es/ESS/bsc-dust-daily-forecast, e-mail: info-services-es@bsc.es). The MACC/CAMS dust profiles are downloaded from the MACC aerosol data base (MACC, 2016). The SKIRON dust profiles can also be provided upon request and are also available at *http://forecast.uoa.gr/dustindx.php*.

Acknowledgements. We thank the R/V Meteor team and German Weather Service (DWD) for their support during the cruise M96. We appreciate the effort of AERONET MAN to equip research vessels with sun photometers for atmospheric research. The SKIRON model operations were supported by the European Commission through the 7th Framework Program MARINA Platform (Marine Renewable Integrated Application Platform, Grant Agreement 241402). NMMB/BSC-Dust model simulations were performed in the MareNostrum supercomputer hosted by BSC. S. Basart acknowledges the CICYT project (CGL2013-46736-R) of the Spanish Government.

Atmos. Chem. Phys. Discuss., https://doi.org/10.5194/acp-2017-502
Manuscript under review for journal Atmos. Chem. Phys.
Discussion started: 12 June 2017

Atmospheric Chemistry and Physics Discussions

References

Alfaro, S. C. and Gomes, L., Modeling mineral aerosol production by wind erosion: Emission intensities and aerosol size distributions in source areas, J. Geophys. Res., 106, 18075–18084, 2001.

Ansmann, A., Wandinger, U., Riebesell, M., Weitkamp, C., and Michaelis, W.: Independent measurement of extinction and backscatter profiles in cirrus clouds by using a combined Raman elastic–backscatter lidar, Appl. Opt., 31, 7113–7131, 1992.

Astitha, M., Kallos, G., and Katsafados, P.: Air pollution modeling in the Mediterranean Region: Analysis and forecasting of episodes, Atmos. Res., 89, 358-364, doi:10.1016/j. atmosres.2008.03.006, 2008

Baars, H., Kanitz, T., Engelmann, R., Althausen, D., Heese, B., Komppula, M., Preißler, J., Tesche, M., Ansmann, A., Wandinger, U., Lim, J.-H., Ahn, J. Y., Stachlewska, I. S., Amiridis, V., Marinou, E., Seifert, P., Hofer, J., Skupin, A., Schneider, F., Bohlmann, S., Foth, A., Bley, S., Pfüller, A., Giannakaki, E., Lihavainen, H., Viisanen, Y., Hooda, R. K., Pereira, S. N., Bortoli, D., Wagner, F., Mattis, I., Janicka, L., Markowicz, K. M., Achtert, P., Artaxo, P., Pauliquevis, T., Souza, R. A. F., Sharma, V. P., van Zyl, P. G., Beukes, J. P., Sun, J., Rohwer, E. G., Deng, R., Mamouri, R.-E., and Zamorano, F.: An overview of the first decade of PollyNET: an emerging network of automated Raman-polarization lidars for continuous aerosol profiling, Atmos. Chem. Phys., 16, 5111-5137, doi:10.5194/acp-16-5111-2016, 2016.

Badia, A. and Jorba, O.: Gas-phase evaluation of the online NMMB/BSC-CTM model over Europe for 2010 in the framework of the AQMEII-Phase2 project, Atmos. Environ., 115, 657–669, doi:10.1016/j.atmosenv.2014.05.055, 2014.

Basart, S., Vendrell, L., Baldasano, J. M.: High-resolution dust modelling over complex terrains in West Asia, Aeolian Research, 23, 37–50, doi:10.1016/j.aeolia.2016.09.005, 2016.

Benedetti, A., Morcrette, J.-J., Boucher, O., Dethof, A, Engelen, R. J., Fisher, M., Flentje, H., Huneeus, N, Jones, L., Kaiser, J. W., Kinne, S., Mangold, A., Razinger, M., Simmons, A. J., and Suttie, M.: Aerosol analysis and forecast in the European Centre for Medium-Range Weather Forecasts Integrated Forecast System: 2. Data assimilation, J. Geophys. Res., 114, D13205, doi:10.1029/2008JD011115, 2009.

Betts, A. K.: A new convective adjustment scheme, Part I: Observational and theoretical basis, Q. J. Roy. Meteor. Soc., 112, 677–691, doi:10.1002/qj.49711247307, 1986.

Betts, A. K. and Miller, M. J.: A new convective adjustment scheme, Part II: Single column tests using GATE wave, BOMEX, ATEX and arctic air-mass data sets, Q. J. Roy. Meteor. Soc., 112, 693–709, doi:10.1002/qj.49711247308, 1986

Binietoglou, I., Basart, S., Alados-Arboledas, L., Amiridis, V., Argyrouli, A., Baars, H., Baldasano, J. M., Balis, D., Belegante, L., Bravo-Aranda, J. A., Burlizzi, P., Carrasco, V., Chaikovsky, A., Comerón, A., D'Amico, G., Filioglou, M., Granados-Muñoz, M. J., Guerrero-Rascado, J. L., Ilic, L., Kokkalis, P., Maurizi, A., Mona, L., Monti, F., Muñoz-Porcar, C., Nicolae, D., Papayannis, A., Pappalardo, G., Pejanovic, G., Pereira, S. N., Perrone, M. R., Pietruczuk, A., Posyniak, M., Rocadenbosch, F., Rodríguez-Gómez, A., Sicard, M., Siomos, N., Szkop, A., Terradellas, E., Tsekeri, A., Vukovic, A., Wandinger, U., and Wagner, J.: A methodology for investigating dust model performance using synergistic EARLINET/AERONET dust concentration retrievals, Atmos. Meas. Tech., 8, 3577-3600, doi:10.5194/amt-8-3577-2015, 2015.

Colarco, P. R., Toon, O. B., Reid, J. S., Livingston, J. M., Russell, P. B., Redemann, J., Schmid, B., Maring, H. B., Savoie, D., Welton, E. J., Campbell, J. R., Holben, B. N., and Levy, R.: Saharan dust transport to the Caribbean during PRIDE: 2. Transport, vertical profiles, and deposition in simulations of in situ and remote sensing observations, J. Geophys. Res., 108, 8590, doi:10.1029/2002JD002659, D19, 2003.

Cuevas, E., Camino, C., Benedetti,A., Basart, S., Terradellas, E., Baldasano, J. M., Morcrette, J. J., Marticorena, B., Goloub, P., Mortier, A., Berjón, A., Hernández, Y., Gil-Ojeda, M., and Schulz, M.: The MACC-II 2007–2008 reanalysis: atmospheric dust evaluation and characterization over northern Africa and the Middle East, Atmos. Chem. Phys., 15, 3991-4024, doi:10.5194/acp-15-3991-2015, 2015.

D'Almeida, G. A.: On the variability of desert aerosol radiative characteristics, J. Geophys. Res., 92, 3017–3026, doi:10.1029/JD092iD03p03017, 1987.

DeMott, P. J., Prenni, A. J., McMeeking, G. R., Sullivan, R. C., Petters, M. D., Tobo, Y., Niemand, M., Möhler, O., Snider, J. R., Wang, Z., and Kreidenweis, S. M.: Integrating laboratory and field data to quantify the immersion freezing ice nucleation activity of mineral dust particles, Atmos. Chem. Phys., 15, 393–409, doi:10.5194/acp-15-393-2015, 2015.

Di Tomaso, E., Schutgens, N. A. J., Jorba, O., and Pérez García-Pando, C.: Assimilation of MODIS Dark Target and Deep Blue observations in the dust aerosol component of NMMB-MONARCH version 1.0, Geosci. Model Dev., 10, 1107-1129, doi:10.5194/gmd-10-1107-2017, 2017.

Engelmann, R., Kanitz, T., Baars, H., Heese, B., Althausen, D., Skupin, A., Wandinger, U., Komppula, M., Stachlewska, I. S., Amiridis, V., Marinou, E., Mattis, I., Linné, H., and Ansmann, A.: The automated multiwavelength Raman polarization and water-vapor lidar PollyXT: the neXT generation, Atmos. Meas. Tech., 9, 1767-1784, doi:10.5194/amt-9-1767-2016, 2016.

Escribano, J., Boucher, O., Chevallier, F., and Huneeus, N.: Impact of the choice of the satellite aerosol optical depth product in a sub-regional dust emission inversion, Atmos. Chem. Phys. Discuss., doi:10.5194/acp-2016-1011, in review, 2017.

Ferrier, B. S., Jin, Y., Lin, Y., Black, T., Rogers, E., and DiMego, G.: Implementation of a new grid-scale cloud and precipitation scheme in the NCEP Eta model, in: Proceedings of the 15th Conf. on Numerical Weather Prediction, vol. 19, Am. Meteor. Soc., San Antonio, TX, USA, 12–16 August 2002, 280–283, 2002.

Gama, C., Tchepel, O., Baldasano, J. M., Basart, S., Ferreira, J., Pio, C., Cardoso, J. and Borrego, C.: Seasonal patterns of Saharan dust over Cape Verde-a combined approach using observations and modelling, Tellus B, 67, 24410, doi:10.3402/tellusb.v67.24410, 2015

Gasch, P., Rieger, D., Walter, C., Khain, P., Levi, Y., and Vogel, B.: An analysis of the September 2015 severe dust event in the Eastern Mediterranean, Atmos. Chem. Phys. Discuss., doi:10.5194/acp-2017-11, in review, 2017.

Gasteiger, J., Wiegner, M., Groß, S., Freudenthaler, V., Toledano, C., Tesche, M., and Kandler, K.: Modelling lidar-relevant optical properties of complex mineral dust aerosols, Tellus B, 63, 725–741, doi:10.1111/j.1600-0889.2011.00559.x, 2011.

Gasteiger, J., Groß, S., Sauer, D., Haarig, M., Ansmann, A., and Weinzierl, B.: Particle settling and vertical mixing in the Saharan Air Layer as seen from an integrated model, lidar, and in situ perspective, Atmos. Chem. Phys., 17, 297-311, doi:10.5194/acp-17-297-2017, 2017.

Ginoux, P., Chin, M., Tegen, I., Prospero, J.M., Holben, B., Dubovik, O., and Lin, S.-J.: Sources and distributions of dust aerosols simulated with the GOCART model, J. Geophys. Res., 106, 20255–20273, doi:10.1029/2000JD000053, 2001.

Groß, S., Tesche, M., Freudenthaler, V., Toledano, C., Wiegner, M., Ansmann, A., Althausen, D., and Seefeldner, M.: Characterization of Saharan dust, marine aerosols and mixtures of biomass-burning aerosols and dust by means of multi-wavelength depolarization and Raman lidar measurements during SAMUM 2, Tellus B, 63, 706-724, doi:10.1111/j.1600-0889.2011.00556.x, 2011.

Haarig, M., Ansmann, A., Althausen, D., Klepel, A., Groß, S., Freudenthaler, V., Toledano, C., Mamouri, R.-E., Farrell, D. A., Prescod, D. A., Marinou, E., Burton, S. P., Gasteiger, J., Engelmann, R., and Baars, H.: Triple-wavelength depolarization-ratio profiling of Saharan dust over Barbados during SALTRACE in 2013 and 2014, Atmos. Chem. Phys. Discuss., doi:10.5194/acp-2017-170, in review, 2017a.

Haarig, M., Ansmann, A., Althausen, D., Gasteiger, J., and Kandler, K.: Linear depolarization ratio of dried marine particles: SALTRACE lidar observations and modeling, Atmos. Chem. Phys., in preparation, 2017b.

Hande, L. B., Engler, C., Hoose, C., and Tegen, I.: Seasonal variability of Saharan desert dust and ice nucleating particles over Europe, Atmos. Chem. Phys., 15, 4389-4397, doi:10.5194/acp-15-4389-2015, 2015.

Hande, L. B., Engler, C., Hoose, C., and Tegen, I.: Parameterizing cloud condensation nuclei concentrations during HOPE, Atmos. Chem. Phys., 16, 12059-12079, doi:10.5194/acp-16-12059-2016, 2016

Haustein, K., Pérez, C., Baldasano, J. M., Jorba, O., Basart, S., Miller, R. L., Janjic, Z., Black, T., Nickovic, S., Todd, M. C., Washington, R., Müller, D., Tesche, M., Weinzierl, B., Esselborn, M. and Schladitz, A.: Atmospheric dust modeling from meso to global scales with the online NMMB/BSC-Dust model-Part 2: Experimental campaigns in Northern Africa, Atmos. Chem. Phys., 12, 2933-2958, doi:10.5194/acp-12-2933-2012, 2012.

Holben, B. N., Eck, T. F., Slutsker, I., Tanré, D., Buis, J. P., Setzer, A., Vermote, E., Reagan, J. A., Kaufman, Y. J., Nakajima, T., Lavenu, F., Jankowiak, I., and Smirnov, A.: AERONET – a federated instrument network and data archive for aerosol characterization, Remote Sens. Environ., 66, 1–16, 1998.

Huneeus, N., Schulz, M., Balkanski, Y., Griesfeller, J., Prospero, J., Kinne, S., Bauer, S., Boucher, O., Chin, M., Dentener, F., Diehl, T., Easter, R., Fillmore, D., Ghan, S., Ginoux, P., Grini, A., Horowitz, L., Koch, D., Krol, M. C., Landing, W., Liu, X., Mahowald, N., Miller, R., Morcrette, J.-J., Myhre, G., Penner, J., Perlwitz, J., Stier, P., Takemura, T., and Zender, C. S.: Global dust model intercomparison in AeroCom phase I, Atmos. Chem. Phys., 11, 7781-7816, doi:10.5194/acp-11-7781-2011, 2011.

Huneeus, N., Chevallier, F., and Boucher, O.: Estimating aerosol emissions by assimilating observed aerosol optical depth in a global aerosol model, Atmos. Chem. Phys., 12, 4585-4606, doi:10.5194/acp-12-4585-2012, 2012.

Huneeus, N., Basart, S., Fiedler, S., Morcrette, J.-J., Benedetti, A., Mulcahy, J., Terradellas, E., Pérez García-Pando, C., Pejanovic, G., Nickovic, S., Arsenovic, P., Schulz, M., Cuevas, E., Baldasano, J. M., Pey, J., Remy, S., and Cvetkovic, B.: Forecasting the northern African dust outbreak towards Europe in April 2011: a model intercomparison, Atmos. Chem. Phys., 16, 4967-4986, doi:10.5194/acp-16-4967-2016, 2016.

Iacono, M. J., Delamere, J. S., Mlawer, E. J., Shephard, M. W., Clough, S. A., and Collins, W. D.: Radiative forcing by long-lived greenhouse gases: Calculations with the AER Radiative transfer models, J. Geophys. Res., 113, D13103, doi:10.1029/2008JD009944, 2008.

Ignatov, A., and Gutman, G.: The derivation of the green vegetation fraction from NOAA/AVHRR data for use in numerical weather prediction models. Int. J. Remote Sens. 19, 1533–1543, doi: 10.1080/014311698215333, 1998.

Janjic, Z.: The Step-Mountain Eta Coordinate Model: Further Developments of the Convection, Viscous Sublayer, and Turbulence Closure Schemes, Mon. Weather Rev., 122, 927–945, doi:10.1175/1520-0493(1994)122<0927:TSMECM>2.0.CO;2, 1994.

Janjic, Z., Janjic, T., and Vasic, R.: A class of conservative fourthorder advection schemes and impact of enhanced formal accuracy on extended-range forecasts, Mon. Weather Rev., 139, 1556–1568, doi:10.1175/2010MWR3448.1, 2011.

Jorba, O. Dabdub, D., Blaszczak-Boxe, C., Pérez García-Pando, C., Janjic, Z., Baldasano, J. M., Spada, M., Badia, A., and Goncalves, M.: Potential significance of photoexcited NO2 on global air quality with the NMMB/BSC chemical transport model, J. Geophys. Res., 117, D13301, doi:10.1029/2012JD017730, 2012.

Kallos, G., Astitha, M., Katsafados, P., and Spyrou, C.: Long-range transport of anthropogenically and naturally produced particulate matter in the Mediterranean and North Atlantic: Current state of knowledge, J. Appl. Meteorol. Climat., 46, 1230–1251, doi: 10.1175/JAM2530.1, 2007.

Kanitz, T., Seifert, P., Ansmann, A., Engelmann, R., Althausen, D., Casiccia, C., and Rohwer, E. G.: Contrasting the impact of aerosols at northern and southern midlatitudes on heterogeneous ice formation, Geophys. Res. Lett., 38, L17802, doi:10.1029/2011GL048532, 2011.

Kanitz, T., Ansmann, A., Engelmann, R., and Althausen, D.: North-south cross sections of the vertical aerosol distribution over the Atlantic Ocean from multiwavelength Raman/polarization lidar during Polarstern cruises J. Geophys. Res. Atmos., 118, 2643-2655, doi:10.1002/jgrd.50273, 2013.

Karyampudi, V. M., Palm, S. P., Reagen, J. A., Fang, H., Grant, W. B., Hoff, R. M., Moulin, C., Pierce, H. F., Torres, O., Browell, E. V., Melfi, S. H.: Validation of the Saharan Dust Plume Conceptual Model Using Lidar, Meteosat, and ECMWF Data, Bull. Amer. Meteor. Soc., 80, 1045-1075, doi:10.1175/1520-0477(1999)080<1045:VOTSDP>2.0.CO;2, 1999.

Kemppinen, O., Nousiainen, T., and Jeong, G. Y.: Effects of dust particle internal structure on light scattering, Atmos. Chem. Phys., 15, 12011-12027, doi:10.5194/acp-15-12011-2015, 2015a.

Kemppinen, O., Nousiainen, T., and Lindqvist, H.: The impact of surface roughness on scattering by realistically shaped wavelength-scale dust particles, J. Quant. Spect. Radiat. Transfer, 150, 55–67, doi:10.1016/j.jqsrt.2014.05.024.

Kim, D., Chin, M., Yu, H., Diehl, T., Tan, Q., Kahn, R. A., Tsigaridis, K., Bauer, S. E., Takemura, T., Pozzoli, L., Bellouin, N., Schulz, M., Peyridieu, S., Chédin, A., and Koffi, B.: Sources, sinks, and transatlantic transport of North African dust aerosol: A multimodel analysis and comparison with remote sensing data, J. Geophys. Res. Atmos., 119, 6259–6277, doi:10.1002/2013JD021099, 2014.

Koffi, B., Schulz, M., Bréon, F.-M., Griesfeller, J., Winker, D. M., Balkanski, Y., Bauer, S., Berntsen, T., Chin, M., Collins, W. D., Dentener, F., Diehl, T., Easter, R. C., Ghan, S. J., Ginoux, P. A., Gong, S., Horowitz, L. W., Iversen, T., Kirkevag, A., Koch, D. M., Krol, M., Myhre, G., Stier, P., and Takemura, T.: Application of the CALIOP layer product to evaluate the vertical distribution of aerosols estimated by global models: Part 1. AeroCom phase I results. J. Geophys. Res., 117, no. D10, D10201, doi:10.1029/2011JD016858, 2012.

Koffi, B., Schulz, M., Bréon, F.-M., Dentener, F., Steensen, B. M., Griesfeller, J., Winker, D., Balkanski, Y., Bauer, S. E., Bellouin, N., Berntsen, T., Bian, H., Chin, M., Diehl, T., Easter, R., Ghan, S., Hauglustaine, D. A., Iversen, T., Kirkevag, A., Liu, X., Lohmann, U., Myhre, G., Rasch, P., Seland, O., Skeie, R. B., Steenrod, S. D., Stier, P., Tackett, J., Takemura, T., Tsigaridis, K., Vuolo, M. R., Yoon, J., and Zhang, K.: Evaluation of the aerosol vertical distribution in global aerosol models through comparison against CALIOP measurements: AeroCom phase II results, J. Geophys. Res. Atmos., 121, 7254–7283, doi:10.1002/2015JD024639, 2016.

Kok, J. F.: A scaling theory for the size distribution of emitted dust aerosols suggests climate models underestimate the size of the global dust cycle, Proc. Natl. Acad. Sci. USA, 108, 1016–1021, doi:10.1073/pnas.1014798108, 2011a.

Kok, J. F.: Does the size distribution of mineral dust aerosols depend on the wind speed at emission?, Atmos. Chem. Phys., 11, 10149-10156, doi:10.5194/acp-11-10149-2011, 2011b.

Kok, J. F., Mahowald, N. M., Fratini, G., Gillies, J. A., Ishizuka, M., Leys, J. F., Mikami, M., Park, M.-S., Park, S.-U., Van Pelt, R. S., and Zobeck, T. M.: An improved dust emission model - Part 1: Model description and comparison against measurements, Atmos. Chem. Phys., 14, 13023-13041, doi:10.5194/acp-14-13023-2014, 2014a.

Kok, J. F., Albani, S., Mahowald, N. M., and Ward, D. S.: An improved dust emission model - Part 2: Evaluation in the Community Earth System Model, with implications for the use of dust source functions, Atmos. Chem. Phys., 14, 13043-13061, doi:10.5194/acp-14-13043-2014, 2014b.

Kok, J. F., Ridley, D. A., Zhou, Q., Miller, R. L., Zhao, C., Heald, C. L., Ward, D. S., Albani, S., and Haustein, K.: Smaller desert dust cooling effect estimated from analysis of dust size and abundance, Nature Geoscience, 10, 274–278, doi:10.1038/ngeo2912, 2017

Lindqvist, H., Jokinen, O., Kandler, K., Scheuvens, D., and Nousiainen, T.: Single scattering by realistic, inhomogeneous mineral dust particles with stereogrammetric shapes, Atmos. Chem. Phys., 14, 143-157, doi:10.5194/acp-14-143-2014, 2014.

MACC model: MACC aerosol data base, available at: data server ECGATE, MARS data base, download by using a script with the specifications: class=mc, dataset=macc_nrealtime, expver=0001, last access: September, 2016.

Marécal, V., Peuch, V.-H., Andersson, C., Andersson, S., Arteta, J., Beekmann, M., Benedictow, A., Bergström, R., Bessagnet, B., Cansado, A., Chéroux, F., Colette, A., Coman, A., Curier, R. L., Denier van der Gon, H. A. C., Drouin, A., Elbern, H., Emili, E., Engelen, R. J., Eskes, H. J., Foret, G., Friese, E., Gauss, M., Giannaros, C., Guth, J., Joly, M., Jaumouillé, E., Josse, B., Kadygrov, N., Kaiser, J. W., Krajsek, K., Kuenen, J., Kumar, U., Liora, N., Lopez, E., Malherbe, L., Martinez, I., Melas, D., Meleux, F., Menut,L., Moinat, P., Morales, T., Parmentier, J., Piacentini, A., Plu, M., Poupkou, A., Queguiner, S., Robertson, L., Rouil, L., Schaap, M., Segers, A., Sofiev, M., Tarasson, L., Thomas, M., Timmermans, R., Valdebenito, Á., van Velthoven, P., van Versendaal, R., Vira, J., and Ung, A.: A regional air quality forecasting system over Europe: the MACC-II daily ensemble production, Geosci. Model Dev., 8, 2777-2813, doi:10.5194/gmd-8-2777-2015, 2015

Mamouri, R. E. and Ansmann, A.: Fine and coarse dust separation with polarization lidar, Atmos. Meas. Tech., 7, 3717-3735, doi:10.5194/amt-7-3717-2014, 2014.

Mamouri, R. E. and Ansmann, A.: Estimated desert-dust ice nuclei profiles from polarization lidar: methodology and case studies, Atmos. Chem. Phys., 15, 3463-3477, doi:10.5194/acp-15-3463-2015, 2015.

Mamouri, R.-E. and Ansmann, A.: Potential of polarization lidar to provide profiles of CCN- and INP-relevant aerosol parameters, Atmos. Chem. Phys., 16, 5905-5931, doi:10.5194/acp-16-5905-2016, 2016.

Mamouri, R.-E., Ansmann, A., Nisantzi, A., Solomos, S., Kallos, G., and Hadjimitsis, D. G.: Extreme dust storm over the eastern Mediterranean in September 2015: satellite, lidar, and surface observations in the Cyprus region, Atmos. Chem. Phys., 16, 13711-13724, doi:10.5194/acp-16-13711-2016, 2016.

Mamouri, R.-E., and Ansmann, A.: Separation of fine-mode dust, coarse-mode dust, and non-dust aerosol components with polarization lidar: Extended POLIPHON methodology for multiple wavelengths Atmos. Meas. Tech., SALTRACE special issue, in preparation, 2017.

Marticorena, B. and Bergametti, G.: Modeling the atmospheric dust cycle: 1. design of a soil-derived dust emission scheme, J. Geophys. Res., 100, 16415–16430, doi:10.1029/95JD00690, 1995.

Marticorena, B., Bergametti, G., Aumont, B., Callot, Y., N'Doumé, C., and Legrand, M.: Modeling the atmospheric dust cycle, 2. simulation of Saharan dust sources, J. Geophys. Res., 102, 4387–4404, doi:10.1029/96JD02964, 1997.

Miller, D. A., and White, R. A.: A conterminous United States multilayer soil characteristics data set for regional climate and hydrology modeling, Earth Interactions, 2, 1–26, doi: http://dx.doi.org/10.1175/1087-3562(1998)002<0001:ACUSMS>2.3.CO;2, 1998

Mlawer, E. J., Taubman, S. J., Brown, P. D., Iacono, M. J., and Clough, S. A.: Radiative transfer for inhomogeneous atmospheres: RRTM, a validated correlated-k model for the longwave, J. Geophys. Res.-Atmos., 102, 16663–16682, doi:10.1029/97JD00237, 1997.

Morcrette, J.-J., Boucher, O., Jones, L., Salmond, D., Bechtold, P., Beljaars, A., Benedetti, A., Bonet, A., Kaiser, J. W., Razinger, M., Schulz, M., Serrar, S., Simmons, A. J., Sofiev, M. Suttie, M., Tompkins, A. M., and Untch, A.: Aerosol analysis and forecast in the European Centre for Medium-Range Weather Forecasts Integrated Forecast System: Forward modeling, J. Geophys. Res., 114, D06206, doi:10.1029/2008JD011235, 2009.

Mona, L., Papagiannopoulos, N., Basart, S., Baldasano, J., Binietoglou, I., Cornacchia, C., and Pappalardo, G.: EARLINET dust observations vs. BSC-DREAM8b modeled profiles: 12-year-long systematic comparison at Potenza, Italy, Atmos. Chem. Phys., 14, 8781–8793, doi:10.5194/acp-14-8781-2014, 2014.

Müller, D., Ansmann, A., Mattis, I., Tesche, M., Wandinger, U., Althausen, D., and Pisani, G.: Aerosol-type-dependent lidar ratios observed with Raman lidar, J. Geophys. Res., 112, D16202, doi:10.1029/2006JD008292, 2007a.

Müller, D., Mattis, I., Ansmann, A., Wandinger, U., Ritter, C., and Kaiser, D.: Multiwavelength Raman lidar observations of particle growth during long-range transport of forest-fire smoke in the free troposphere, Geophys. Res. Lett., 34, L05803, doi:10.1029/2006GL027936, 2007b.

Nabat, P., Solmon, F., Mallet, M., Kok, J. F., and Somot, S.: Dust emission size distribution impact on aerosol budget and radiative forcing over the Mediterranean region: a regional climate model approach, Atmos. Chem. Phys., 12, 10545-10567, doi:10.5194/acp-12-10545-2012, 2012.

Nickovic, S., Kallos, G., Papadopoulos, A., and Kakaliagou, O.: A model for prediction of desert dust cycle in the atmosphere, J. Geophys. Res., 106, 18113–18130, doi: 10.1029/2000JD900794, 2001.

Nickovic, S., Cvetkovic, B., Madonna, F., Rosoldi, M., Pejanovic, G., Petkovic, S., and Nikolic, J.: Cloud ice caused by atmospheric mineral dust – Part 1: Parameterization of ice nuclei concentration in the NMME-DREAM model, Atmos. Chem. Phys., 16, 11367-11378, doi:10.5194/acp-16-11367-2016, 2016.

Nicoll, K. A., Harrison, R. G., and Ulanowski, Z., Observations of Saharan dust layer electrification, Environ. Res. Lett., 6, 014001, doi:10.1088/1748-9326/6/1/014001, 2011.

Pappalardo, G., Amodeo, A., Apituley, A., Comeron, A., Freudenthaler, V., Linné, H., Ansmann, A., Bösenberg, J., DÁmico, G., Mattis, I., Mona, L., Wandinger, U., Amiridis, V., Alados- Arboledas, L., Nicolae, D., and Wiegner, M.: EARLINET: towards an advanced sustainable European aerosol lidar network, Atmos. Meas. Tech., 7, 2389-2409, doi:10.5194/amt-7-2389- 2014, 2014.

Pérez C., Nickovic, S., Baldasano, J. M., Sicard, M., Rocadenbosch, F., and Cachorro, V. E.: A long Saharan dust event over the western Mediterranean: Lidar, Sun photometer observations, and regional dust modelling, J. Geophys. Res., 111, D15214, doi:10.1029/2005JD006579, 2006.

Pérez, C., Haustein, K., Janjic, Z., Jorba, O., Huneeus, N., Baldasano, J.M., Black, T., Basart, S., Nickovic, S., Miller, R.L., Perlwitz, J., Schulz, M. and Thomson, M.: An online mineral dust aerosol model for meso to global scales: Model description, annual simulations and evaluation, Atmos. Chem. Phys., 11, 13001-13027, doi: 10.5194/acp-11-13001-2011, 2011.

Reddy, M. S., Boucher, O., Bellouin, N., Schulz, M., Balkanski, Y., Dufresne, J.-L., and Pham, M.: Estimates of global multi-component aerosol optical depth and direct radiative perturbation in the Laboratoire de Météorologie Dynamique general circulation model, J. Geophys. Res., 110, D10S16, doi:10.1029/2004JD004757, 2005.

Remer, L. A., Kaufman, Y. J. M, Tanré, D., Mattoo, S., Chu, D. A., Martins, J. V., Li, R.-R., Ichoku, C., Levy, R. C., Kleidman, R. G., Eck, T. F., Vermote, E., and Holben, B. N.: The MODIS Aerosol Algorithm, Products, and Validation, J. Atmos. Sci., 62, 947-973, doi:10.1175/JAS3385.1, 2005.

Ridley, D. A., Heald, C. L., Kok, J. F., and Zhao, C.: An observationally constrained estimate of global dust aerosol optical depth, Atmos. Chem. Phys., 16, 15097-15117, doi:10.5194/acp-16-15097-2016, 2016.

Rittmeister, F., Ansmann, A., Engelmann, R., Skupin, A., Baars, H., Kanitz, T., and Kinne, S.: From the Caribbean to West Africa: Four weeks of continuous dust and marine aerosol profiling with shipborne polarization/Raman lidar - a contribution to SALTRACE, Atmos. Chem. Phys. Discuss., doi:10.5194/acp-2017-130, in review, 2017

Ryder, C. L., Highwood, E. J., Lai, T. M., Sodemann, H., and Marsham, J. H.: Impact of atmospheric transport on the evolution of microphysical and optical properties of Saharan dust, Geophys. Res. Lett., 40, 2433–2438, doi:10.1002/Grl.50482, 2013.

Scanza, R. A., Mahowald, N., Ghan, S., Zender, C. S., Kok, J. F., Liu, X., Zhang, Y., and Albani, S.: Modeling dust as component minerals in the Community Atmosphere Model: development of framework and impact on radiative forcing, Atmos. Chem. Phys., 15, 537-561, doi:10.5194/acp-15-537-2015, 2015.

Shao, Y.: A model for mineral dust emission, J. Geophys. Res., 106, 20239–20254, 2001.

Shao, Y. P.: Simplification of a dust emission scheme and comparison with data, J. Geophys. Res., 109, D10202, doi:10.1029/2003JD004372, 2004.

Shimizu, A., Sugimoto, N., Matsui, I., Arao, K., Uno, I., Murayama, T., Kagawa, N., Aoki, K., Uchiyama, A., and Yamazaki, A.: Continuous observations of Asian dust and other aerosols by polarization lidars in China and Japan during ACE–Asia, J. Geophys. Res., 109, doi:10.1029/2002JD003253, 2004.

Solomos, S., Ansmann, A., Mamouri, R.-E., Binietoglou, I., Patlakas, P., Marinou, E., and Amiridis, V.: Remote sensing and modeling analysis of the extreme dust storm hitting Middle East and Eastern Mediterranean in September 2015, Atmos. Chem. Phys. Discuss., doi:10.5194/acp-2016-1006, in review, 2016.

Spada, M., Jorba, O., Pérez García-Pando, C., Janjic, Z., and Baldasano, J. M.: Modeling and evaluation of the global sea-salt aerosol distribution: sensitivity to size-resolved and sea-surface temperature dependent emission schemes, Atmos. Chem. Phys., 13, 11735–11755, doi:10.5194/acp-13-11735-2013, 2013.

Spyrou, C., Mitsakou, C., Kallos, G., Louka, P., and Vlastou, G.: An improved limited area model for describing the dust cycle in the atmosphere, J. Geophys. Res., 115, D17211, doi:10.1029/2009JD013682, 2010.

Spyrou, C., Kallos, G., Mitsakou, C., Athanasiadis, P., Kalogeri, C., and Iacono, M. J.: Modeling the radiative effects of desert dust on weather and regional climate, Atmos. Chem. Phys., 13, 5489-5504, doi:10.5194/acp-13-5489-2013, 2013.

Sugimoto, N., Uno, I., Nishikawa, M., Shimizu, A., Matsui, I., Dong, X., Chen, Y., and Quan, H.: Record heavy Asian dust in Beijing in 2002: Observations and model analysis of recent events, Geophys. Res. Lett., 30, doi:10.1029/2002GL016349, 2003.

Tegen, I. and Lacis, A. A.: Modelling of particle size distribution and its influence on the radiative properties of mineral dust aerosol, J. Geophys. Res., 101, 19237–19244, doi:10.1029/95JD03610, 1996,

Tegen, I., Harrison, S. P., Kohfeld, K., Prentice, I. C., Coe, M., and Heimann, M.: Impact of vegetation and preferential source areas on global dust aerosol: results from a model study, J. Geophys. Res., 107, 4576, doi:10.1029/2001JD000963, 2002.

Tesche, M., Ansmann, A., Müller, D., Althausen, D., Engelmann, R., Freudenthaler, V., and Groß, S.: Vertically resolved separation of dust and smoke over Cape Verde using multiwavelength Raman and polarization lidars during Saharan Mineral Dust Experiment 2008, J. Geophys. Res., 114, D13202, doi:10.1029/2009JD011862, 2009a.

Tesche, M., Groß, S., Ansmann, A., Müller, D., Althausen, D., Freudenthaler, V., and Esselborn, M.: Profiling of Saharan dust and biomass-burning smoke with multiwavelength polarization Raman lidar at Cape Verde, Tellus B, 63, 649–676, doi:10.1111/j.1600-0889.2011.00548.x, 2011.

Ulanowski, Z., Bailey, J., Lucas, P. W., Hough, J. H., and Hirst, E.: Alignment of atmospheric mineral dust due to electric field, Atmos. Chem. Phys., 7, 6161-6173, doi:10.5194/acp-7-6161-2007, 2007.

Wagner, A., Blechschmidt, A.-M., Bouarar, I., Brunke, E.-G., Clerbaux, C., Cupeiro, M., Cristofanelli, P., Eskes, H., Flemming, J., Flentje, H., George, M., Gilge, S., Hilboll, A., Inness, A., Kapsomenakis, J., Richter, A., Ries, L., Spangl, W., Stein, O., Weller, R., and Zerefos, C.: Evaluation of the MACC operational forecast system - potential and challenges of global near-real-time modelling with respect to reactive gases in the troposphere, Atmos. Chem. Phys., 15, 14005-14030, doi:10.5194/acp-15-14005-2015, 2015

Weinzierl, B., Ansmann, A, Prospero, J. M., Althausen, D., Benker, N., Chouza, F., Dollner, M., Farrell, D., Fomba, W. K., Freudenthaler, V., Gasteiger, J., Groß, S., Haarig, M., Heinold, B., Kandler, K., Kristensen, T. B., Mayol-Bracero, O.-L., Müller, T., Reitebuch, O., Sauer, D., Schäfler, A., Schepanski, K., Tegen, I., Toledano, C., Walser, A.: The Saharan Aerosol Long-range TRansport and Aerosol Cloud Interaction Experiment (SALTRACE): overview and selected highlights, Bull. American. Meteorol. Soc., 2017.

White, B. R.: Soil transport by winds on Mars, J. Geophys. Res., 84, 4643–4651, doi:10.1029/JB084iB09p04643, 1979.

Yang, W., Marshak, A., Kostinski, A. B., and Várnai, T.: Shape-induced gravitational sorting of Saharan dust during transatlantic voyage: Evidence from CALIOP lidar depolarization measurements, Geophys. Res. Lett., 40, 3281–3286, doi:10.1002/grl.50603, 2013.

Zhang, L., Gong, S., Padro, J., and Barrie, L.: A size-segregated particle dry deposition scheme for an atmospheric aerosol module, Atmos. Environ., 35, 549–560, doi:10.1016/S1352-2310(00)00326-5, 2001.

Zhao, C., Chen, S., Leung, L. R., Qian, Y., Kok, J. F., Zaveri, R. A., and Huang, J.: Uncertainty in modeling dust mass balance and radiative forcing from size parameterization, Atmos. Chem. Phys., 13, 10733-10753, doi:10.5194/acp-13-10733-2013, 2013.

Atmos. Chem. Phys. Discuss., https://doi.org/10.5194/acp-2017-502
Manuscript under review for journal Atmos. Chem. Phys.
Discussion started: 12 June 2017

Atmospheric Chemistry and Physics Discussions

Table 1. Size bins (radius intervals) considered in the dust forecast models MACC/CAMS, SKIRON and NMMB/BSC-Dust

Model	fine dust size bins	coarse dust size bins
MACC/CAMS	0.03–0.55 μm	0.55–0.9 μm
		0.9–20 μm
NMMB/BSC-Dust, SKIRON	0.1–0.18 μm	0.6–1.0 μm
	0.18–0.3 μm	1.0–1.8 μm
	0.3–0.6 μm	1.8–3.0 μm
		3.0–6.0 μm
		6.0–10.0 μm

Atmos. Chem. Phys. Discuss., https://doi.org/10.5194/acp-2017-502
Manuscript under review for journal Atmos. Chem. Phys.
Discussion started: 12 June 2017

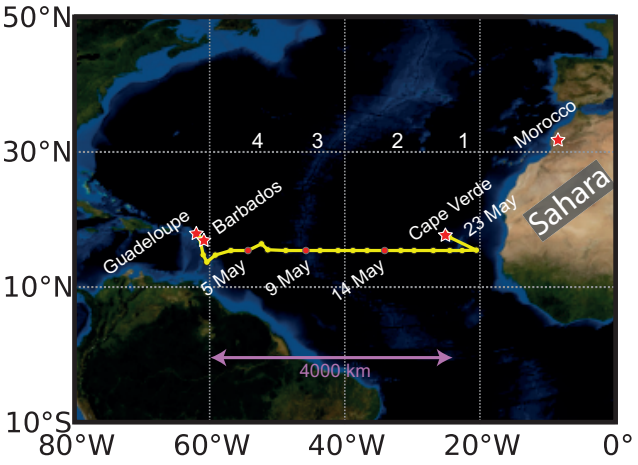

Figure 1. The cruise track of the R/V Meteor from Guadeloupe (29 April 2013) to Cabo Verde (23 May 2013) indicated as a yellow line (Rittmeister et al., 2017). Lidar observations 1–4 (see red circles and star at Cabo Verde) representing key stages of dust layering over the remote Atlantic are discussed in detail in part one (Rittmeister et al., 2017) and are compared with simulated dust profiles in Sect. 3. The locations of the lidar observations are 1000 km (case 1, 23 May 2013, 03:45–05:00 UTC), 1700 km (case 2, 14 May 2013, 23:45–00:20 UTC), 3300 km (case 3, 9 May 2013, 23:15–24:00 UTC), and 4300 km (case 4, 5 May 2013, 23:40–00:35 UTC) west of the African coast.

Atmos. Chem. Phys. Discuss., https://doi.org/10.5194/acp-2017-502
Manuscript under review for journal Atmos. Chem. Phys.
Discussion started: 12 June 2017

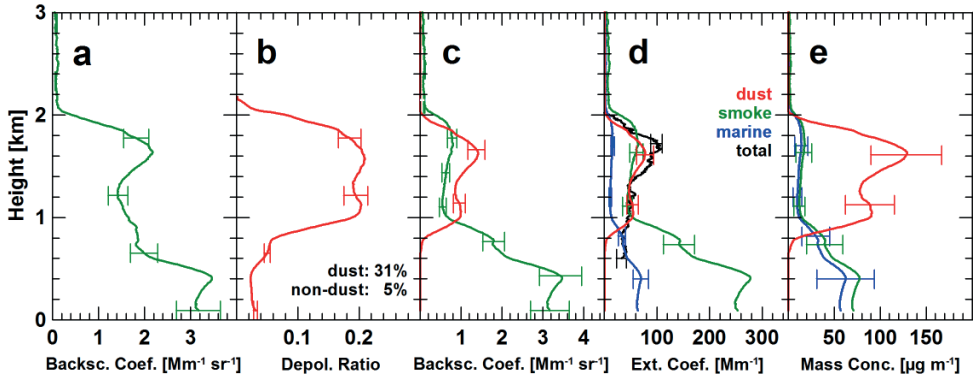

Figure 2. Shipborne lidar observations of the Saharan air layer (SAL, 800–2000 m height) above the marine aerosol layer (MAL) on 5–6 May 2013, 23:40–00:35 UTC (see Fig. 1, case 4): (a) 532 nm particle backscatter coefficient, (b) 532 nm particle linear depolarization ratio, (c) non–dust (green) and dust (red) particle backscatter coefficients, (d) dust extinction coefficient (red) and non-dust extinction coefficients (blue, if the non-dust component is of marine origin, lidar ratio of 20 sr; green, if the aerosol component is, e.g., biomass burning smoke and anthropogenic haze, lidar ratio of 50 sr), and (e) dust (red) and non–dust mass concentration (blue, if marine, green if smoke and haze). Error bars indicate the retrieval uncertainties (one standard deviation). The black curve in (d) it the total particle extinction coefficient independently determined by means of the Raman lidar method.

Atmos. Chem. Phys. Discuss., https://doi.org/10.5194/acp-2017-502
Manuscript under review for journal Atmos. Chem. Phys.
Discussion started: 12 June 2017

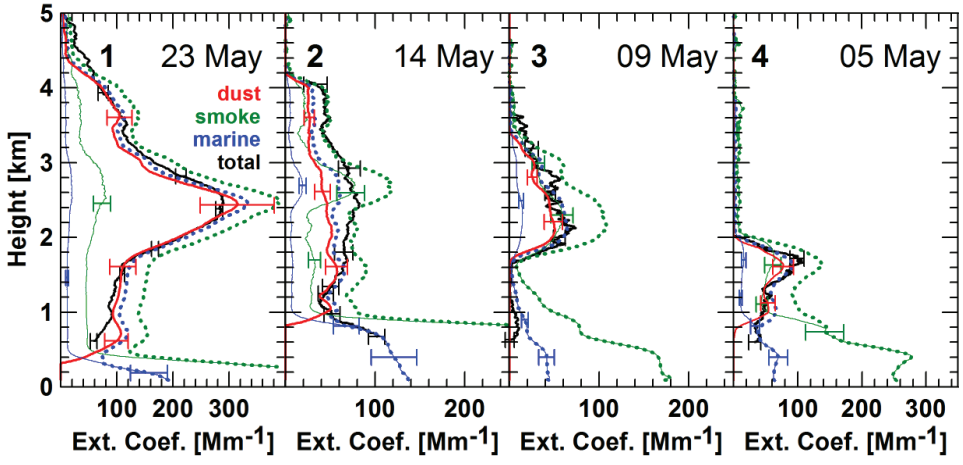

Figure 3. The Saharan aerosol layer as a function of distance from Africa (see Fig. 1, cases 1–4). Shown are the 532 nm particle extinction coefficient measured with Raman lidar (black curves) on 5–6 May, 23:40–00:35 UTC (case 4), 9 May, 23:15–24:00 UTC (case 3), 14–15 May, 23:45–00:20 UTC (case 2), and (d) 23 May 2013, 03:45–05:00 UTC (case 1), and the extinction contributions by desert dust (red solid line) and marine (blue solid line, lidar ratio of 20 sr) or smoke and haze particles (green solid line, lidar ratio of 50 sr). The sum of dust and non-dust extinction contributions are given as thick dotted lines. If the black extinction curve is close to the blue dotted line the non-dust aerosol component is probably of maritime origin (case 1,3,4), in the case that the black and green dotted lines match, the non-dust aerosol component is most likely of anthropogenic origin (upper part in case 2).

Atmos. Chem. Phys. Discuss., https://doi.org/10.5194/acp-2017-502
Manuscript under review for journal Atmos. Chem. Phys.
Discussion started: 12 June 2017

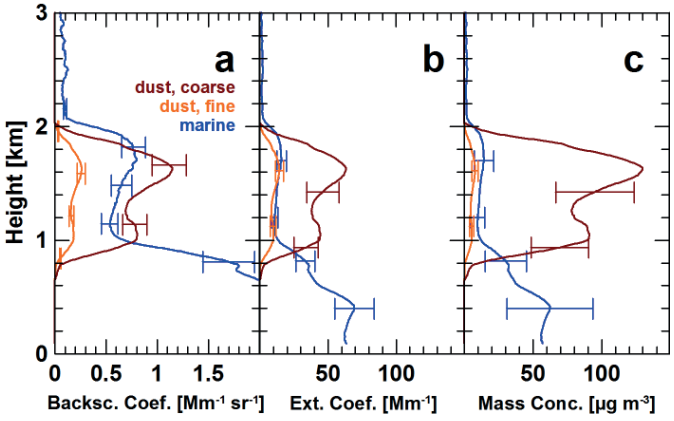

Figure 4. Solutions of the 2-step POLIPHON data analysis (for case 4):(a) non–dust (blue, here for marine aerosol with lidar ratio of 20 sr), fine-mode dust (orange) and coarse-mode dust (dark red) backscatter coefficients, (b) respective marine, fine-mode, and coarse-mode dust extinction coefficients, and (c) marine, fine-mode and coarse-mode dust particle mass concentration. Error bars indicate the retrieval uncertainties (one standard deviation).

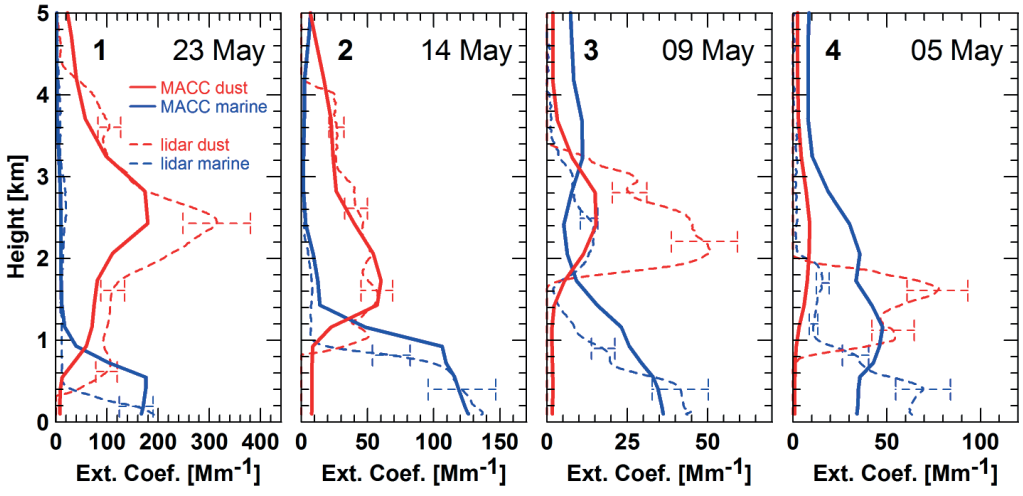

Figure 5. MACC/CAMS simulated marine (blue solid) and dust (red solid) contributions to particle extinction coefficient versus respective lidar observations (dashed blue and red lines) for cases 1–4. Error bars show the overall retrieval uncertainty in the lidar observations. The variability in the modeled dust profiles around R/V Meteor are estimated to be 20-30% (case 1), 10-20% (case 2), 50-80% (case 3), and 20-30% (case 4, see text for more details).

Atmos. Chem. Phys. Discuss., https://doi.org/10.5194/acp-2017-502
Manuscript under review for journal Atmos. Chem. Phys.
Discussion started: 12 June 2017

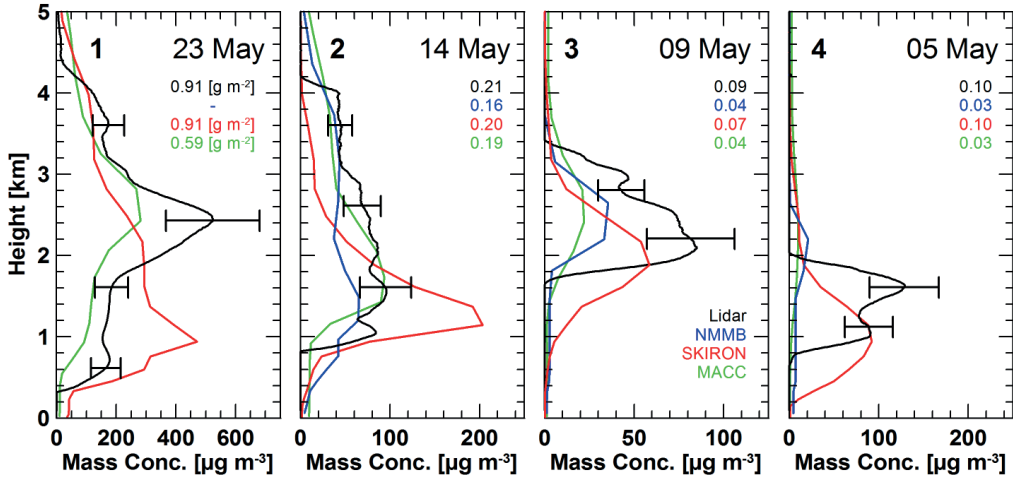

Figure 6. Dust mass concentration profiles observed with lidar (black, with retrieval uncertainty bars) and simulated with NMMB/BSC-Dust (blue), SKIRON (red), and MACC/CAMS (green) for cases 1–4. Column-integrated dust mass concentrations are given as numbers.

Atmos. Chem. Phys. Discuss., https://doi.org/10.5194/acp-2017-502
Manuscript under review for journal Atmos. Chem. Phys.
Discussion started: 12 June 2017

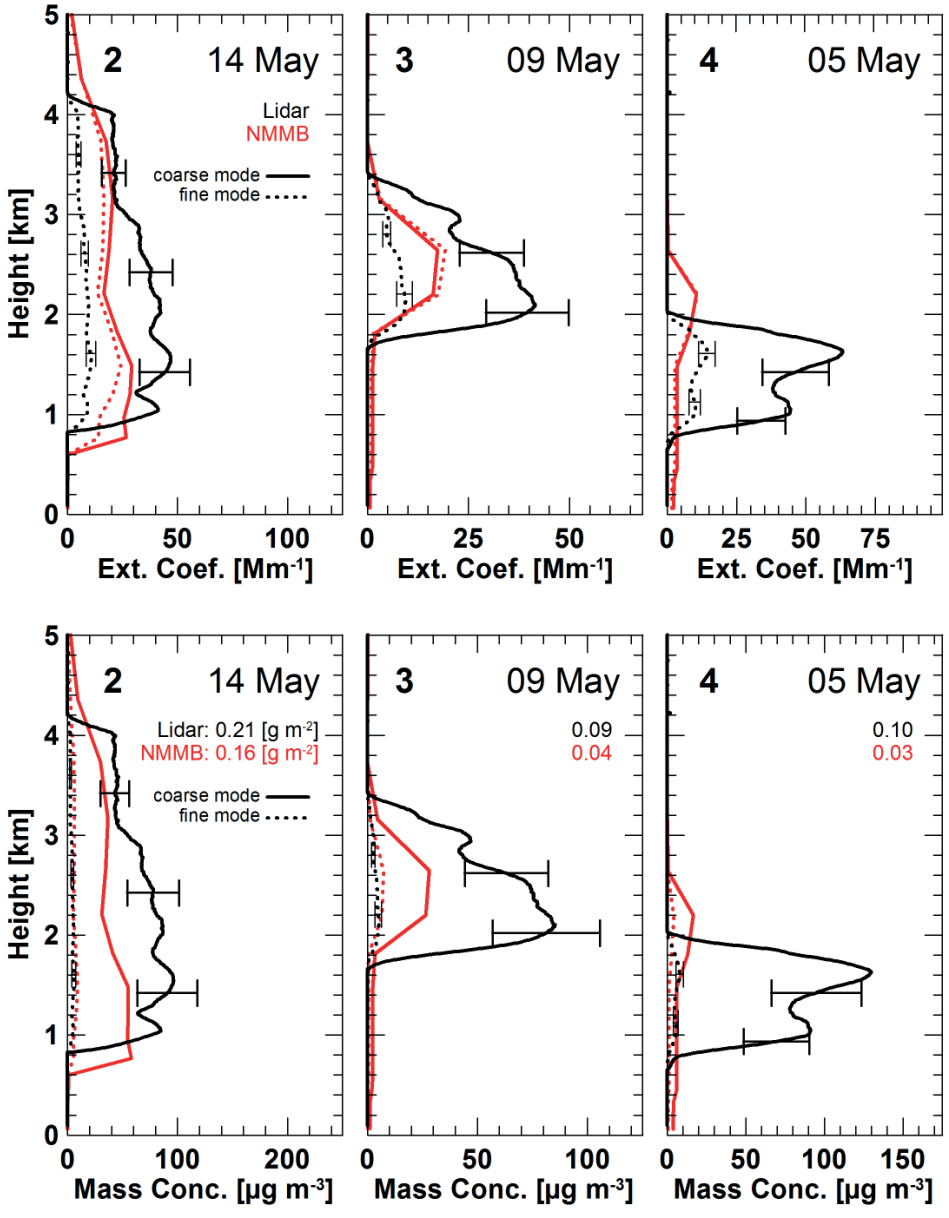

Figure 7. (Top) Comparison fine (dotted) and coarse (solid) dust extinction coefficients derived from lidar observations (black) and simulated with NMMB/BSC-Dust (red). (Bottom) Respective fine (dotted) and coarse (solid) dust mass concentrations derived from the lidar measurements (black) and simulated with NMMB/BSC-Dust (red). Column-integrated total dust mass concentrations are given as numbers. NMMB/BSC-Dust profiles are not available for case 1.

Atmos. Chem. Phys. Discuss., https://doi.org/10.5194/acp-2017-502
Manuscript under review for journal Atmos. Chem. Phys.
Discussion started: 12 June 2017

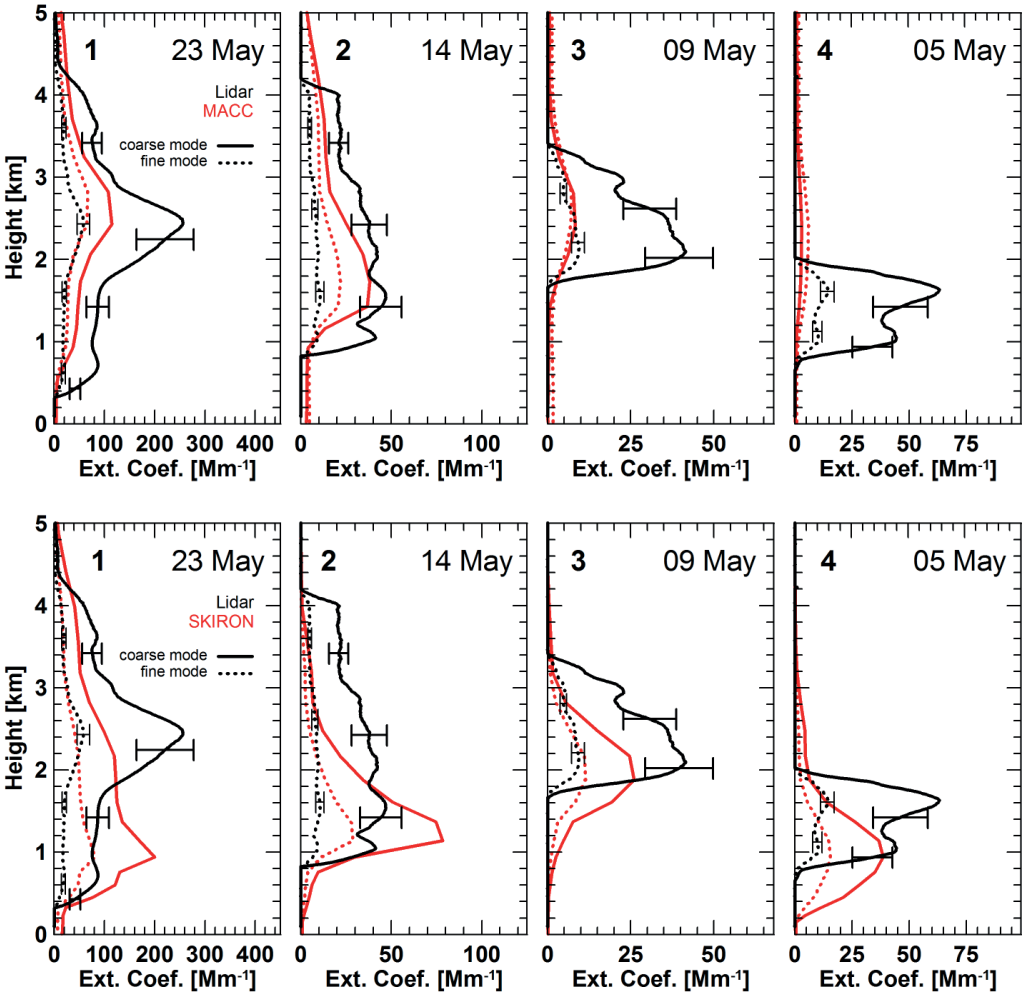

Figure 8. Same as Fig. 7 top, except for comparison with MACC/CAMS simulations (top) and SKIRON (bottom) for all four cases.